Chapter 1
Introduction to Complex Fluids

Alexander Morozov and Saverio E. Spagnolie

Abstract In this chapter we introduce the fundamental concepts in Newtonian and complex fluid mechanics, beginning with the basic underlying assumptions in continuum mechanical modeling. The equations of mass and momentum conservation are derived, and the Cauchy stress tensor makes its first of many appearances. The Navier–Stokes equations are derived, along with their inertialess limit, the Stokes equations. Models used to describe complex fluid phenomena such as shear-dependent viscosity and viscoelasticity are then discussed, beginning with generalized Newtonian fluids. The Carreau–Yasuda and power-law fluid models receive special attention, and a mechanical instability is shown to exist for highly shear-thinning fluids. Differential constitutive models of viscoelastic flows are then described, beginning with the Maxwell fluid and Kelvin–Voigt solid models. After providing the foundations for objective (frame-invariant) derivatives, the linear models are extended to mathematically sound nonlinear models including the upper-convected Maxwell and Oldroyd-B models and others. A derivation of the upper-convected Maxwell model from the kinetic theory perspective is also provided. Finally, normal stress differences are discussed, and the reader is warned about common pitfalls in the mathematical modeling of complex fluids.

1 Introduction

The complexity of biological systems is extraordinary and, from a mathematical modeling point of view, daunting. Even the continuum approximations that give rise to the classical equations of fluid and solid mechanics do not survive the intricacy

A. Morozov
SUPA, School of Physics & Astronomy, University of Edinburgh, JCMB, King's Buildings, Mayfield Road, Edinburgh EH9 3JZ, UK
e-mail: Alexander.Morozov@ed.ac.uk

S.E. Spagnolie (✉)
Department of Mathematics, University of Wisconsin-Madison, 480 Lincoln Dr., Madison, WI 53706, USA
e-mail: spagnolie@math.wisc.edu

© Springer Science+Business Media New York 2015

S.E. Spagnolie (ed.), *Complex Fluids in Biological Systems*, Biological and Medical Physics, Biomedical Engineering,
DOI 10.1007/978-1-4939-2065-5_1

of biological matter, and the systems of equations describing the relevant flows, deformations, and stresses are coupled and nonlinear. This book will be concerned with the dynamics of these complex fluid flows in relation to a number of important biological systems. Many of the biological fluids to be discussed are far from homogeneous. Highly heterogeneous biological materials include mucus, which forms a three-dimensional network with a potentially fractal length-scale distribution, and the cytoskeleton, which is an active structure that undergoes continuous remodeling in response to external and internal stimulation. Nevertheless, with the introduction of a more involved microstructure, such as the inclusion of long chain molecules (e.g., DNA, proteins, microtubules, etc.), continuum assumptions are commonly made to make mathematical modeling and analysis possible. Continuum modeling is even possible when each fundamental parcel includes numerous active particles such as swimming microorganisms, which allows for the derivation of partial differential equations describing *active suspensions*. As will be seen in the chapters to come, the continuum approach has already been an enormously successful method for modeling and understanding real biological systems.

In this first chapter we will lay out the mathematical framework of continuum mechanics and present common constitutive laws used to describe fluids with such properties as shear-dependent viscosity and viscoelasticity. The chapter is organized as follows. We begin with an introduction to the classical equations of Newtonian fluid mechanics in Sect. 2, covering material and spatial descriptions of variables, the mathematization of physical conservation laws, stress, the Navier–Stokes equations, and dimensional analysis. In Sect. 3 we take a first step away from the classical Newtonian constitutive law into elementary models of complex fluids where the viscosity depends on the local flow rate, so-called generalized Newtonian fluids, which include the power-law and Carreau–Yasuda models. More advanced differential constitutive models are the topic of Sect. 4, beginning with the linearly viscoelastic Maxwell fluid and Kelvin–Voigt solid models. After a discussion about objectivity (frame-invariance), the upper-convected Maxwell (UCM), Oldroyd-B, and many other models of nonlinear viscoelastic flow are introduced. A derivation of the UCM model from the perspective of kinetic theory is also provided. In Sect. 5, the material properties of viscoelastic fluids are discussed, and in particular we introduce normal stress differences and describe some of the classical rheological flows that are used to measure the various complex responses to deformation in real fluids. We conclude with a few words of caution about common but ill-advised choices made in the mathematical modeling of complex fluids in Sect. 6, and closing remarks in Sect. 7.

2 Newtonian Fluid Mechanics

The problems to be described in the chapters to come are extraordinarily involved when viewed at the molecular level. The basic mathematical idealization of a homogeneous liquid such as pure water assumes that the fundamental elements

describing the material are *parcels* only somewhat larger than the molecular mean free path. Quantities such as density and pressure in the fluid are assumed to be constant throughout each such volume, but the parcel size is small enough so that the variations in such variables in neighboring parcels are effectively continuous. Partial differential equations modeling the response of a solid or fluid (or a material with both solid-like and fluid-like responses to deformations) are made possible by this *continuum approximation*.

The analysis of classical fluid flows has been one of the great successes of applied mathematics since the time of the Bernoullis, and there are countless excellent presentations of the subject. The reader is referred to the comprehensive texts by Batchelor [1], Landau and Lifshitz [2], Leal [3], and Pozrikidis [4] and the more concise introductions by Acheson [5] and Childress [6]. Here we introduce the basic concepts of mathematical fluid mechanics which, upon the application of mass and momentum conservation laws and specification of a particular constitutive law, result in the Navier–Stokes equations of classical Newtonian flow.

2.1 Material (Lagrangian) and Spatial (Eulerian) Variables

We begin by introducing two important descriptions of independent variables such as density, velocity, and pressure. The first is the material description, also known as the *Lagrangian* description, in which parcels of fluid (or other material) are associated with a "label" $\mathbf{a}$, commonly chosen to be the initial position of the parcel in space. The pressure, for instance, measured at a parcel of material as it moves through space may be written at time t as $P(\mathbf{a},t)$. The second is the spatial description, also known as the *Eulerian* description, in which the same variables are described in terms of a fixed position $\mathbf{x}$ in space, e.g., $P(\mathbf{a},t) = p(\mathbf{x}(\mathbf{a},t),t)$.

The relationship between the two descriptions is a map χ of each label $\mathbf{a}$ in the reference configuration to its current position, $\mathbf{x} = \chi(\mathbf{a},t)$, as illustrated in Fig. 1.1.

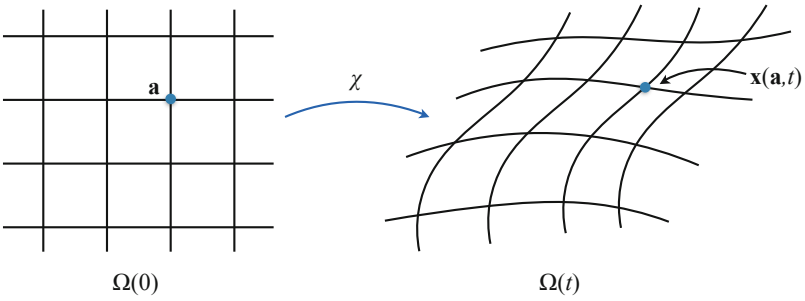

Fig. 1.1 The reference (*Lagrangian*) configuration is deformed to the current (*Eulerian*) configuration at a time t. The material "label" $\mathbf{a}$ maps to a new spatial position $\mathbf{x} = \chi(\mathbf{a},t)$, where $\chi(\mathbf{a},0) = \mathbf{a}$

A control volume in the reference domain $\Omega(0)$ maps to a volume in the current configuration, $\Omega(t)$. Defining the velocity of material at a point $\mathbf{x}$ in space as $\mathbf{u}(\mathbf{x},t)$, then the velocity of a material point labeled by $\mathbf{a}$ is given by

$$\left.\frac{d\mathbf{x}}{dt}\right|_{\mathbf{a}} = \frac{d}{dt}\chi(\mathbf{a},t) = \mathbf{u}(\mathbf{x}(\mathbf{a},t),t), \tag{1.1}$$

where $\mathbf{x}(\mathbf{a},0) = \mathbf{a}$. Similarly, the time rate of change of a scalar variable F in the material description is given simply as $\partial_t F(\mathbf{a},t)$. However, if F is described instead in terms of the spatial variables, $F(\mathbf{a},t) = f(\mathbf{x}(\mathbf{a},t),t)$, then the derivative must correct for the change of frame, and instead (using the chain rule) we find

$$\left.\frac{d}{dt}f(\mathbf{x}(\mathbf{a},t),t)\right|_{\mathbf{a}} = \frac{\partial f}{\partial t} + \frac{\partial f}{\partial x_i}\frac{\partial x_i}{\partial t} = (\partial_t + \mathbf{u}\cdot\nabla)f = \frac{Df}{Dt}. \tag{1.2}$$

We have used the Einstein summation notation where a summation is implied over the repeated index i. The operator $D/Dt = \partial_t + \mathbf{u}\cdot\nabla$ is the *material derivative*, which is a time derivative that follows the material as it deforms. The acceleration of a fluid particle, written in terms of the spatial representation of the velocity field $\mathbf{u}(\mathbf{x},t)$, is then given by

$$\frac{D\mathbf{u}}{Dt} = \frac{\partial \mathbf{u}}{\partial t} + \mathbf{u}\cdot\nabla\mathbf{u}. \tag{1.3}$$

Finally, an important measure of the fluid deformation is the Jacobian matrix of the map $\mathbf{x} = \chi(\mathbf{a},t)$, also known as the *deformation gradient tensor*, given by $\mathbf{F} = \partial\mathbf{x}/\partial\mathbf{a}$ (where $F_{ij} = \partial x_i/\partial a^j$), and $\mathbf{F}(\mathbf{x},0) = \mathbf{I}$, the identity operator. For instance, a line element $d\mathbf{a}$ from one material point to another in the reference configuration transforms to a new line element $d\mathbf{x}$ in the current configuration as $d\mathbf{x} = \mathbf{F}\cdot d\mathbf{a}$. As we proceed to consider conservation laws of mass and momentum we will require the time derivative of the determinant of the deformation gradient tensor $J = \det\mathbf{F}$, which is given by

$$\frac{dJ}{dt} = (\nabla\cdot\mathbf{u})J, \tag{1.4}$$

(see [6]). A volume-preserving or *incompressible* material is one for which $J(\mathbf{x},t) = 1$ and hence $\nabla\cdot\mathbf{u} = 0$ for all $\mathbf{x}$ and t. All of the fluids considered in this book are treated as incompressible.

2.2 Conservation of Mass

The density of a fluid, $\rho(\mathbf{x},t)$, is defined as the mass per volume in an infinitesimal fluid parcel centered at $\mathbf{x}$. Consider a material volume $\Omega(t)$ in the current configuration. As the material volume moves and deforms under the flow, the mass

of fluid in $\Omega(t)$ is determined by integrating the density throughout the volume, $M(t) = \int_{\Omega(t)} \rho(\mathbf{x},t)\,dV$. Absent the creation or destruction of mass, we will then have that the mass in the material volume at any time is equal to its initial value, $M(t) = M(0)$ or $dM/dt = 0$. Mass conservation may then be written in the Eulerian form as

$$\frac{d}{dt}\int_{\Omega(t)} \rho(\mathbf{x},t)\,dV_x = 0, \tag{1.5}$$

with $dV_x = dx_1\,dx_2\,dx_3$. A differential form of mass conservation is achieved by first representing the density in the material coordinates,

$$\begin{aligned} 0 = \frac{d}{dt}\int_{\Omega(t)} \rho(\mathbf{x},t)\,dV_x &= \frac{d}{dt}\int_{\Omega(0)} \rho(\mathbf{x}(\mathbf{a},t),t) J\,dV_a \\ &= \int_{\Omega(0)} \left(\frac{D\rho}{Dt}(\mathbf{x}(\mathbf{a},t),t) + \rho(\mathbf{x}(\mathbf{a},t),t)(\nabla\cdot\mathbf{u})\right) J\,dV_a \\ &= \int_{\Omega(t)} \left(\frac{D\rho}{Dt}(\mathbf{x},t) + \rho(\mathbf{x},t)(\nabla\cdot\mathbf{u})\right) dV_x. \end{aligned} \tag{1.6}$$

This relation is a special case of the Reynolds transport theorem, or convection theorem, as applied to the scalar function $\rho(\mathbf{x},t)$. Since the above holds for all material volumes, we arrive at a differential form of mass conservation:

$$\frac{D\rho}{Dt} + \rho(\nabla\cdot\mathbf{u}) = 0. \tag{1.7}$$

In the event that the fluid is incompressible, $\nabla\cdot\mathbf{u} = 0$, so that $D\rho/Dt = 0$. In other words, in an incompressible flow, the density associated with any material point remains constant as it moves with the fluid.

2.3 Conservation of Momentum

While the mass in a control volume is given by the integrated fluid density, the fluid momentum contained in a volume $\Omega(t)$ may be written in terms of Eulerian variables as $\mathbf{p}(t) = \int_{\Omega(t)} \rho(\mathbf{x},t)\mathbf{u}(\mathbf{x},t)\,dV_x$. In a similar calculation as in the previous section and using Eq. (1.7), we have the following identity:

$$\begin{aligned} \frac{d}{dt}\mathbf{p}(t) = \frac{d}{dt}\int_{\Omega(t)} (\rho\mathbf{u})(\mathbf{x},t)\,dV_x &= \frac{d}{dt}\int_{\Omega(0)} (\rho\mathbf{u})(\mathbf{x}(\mathbf{a},t),t) J\,dV_a \\ &= \int_{\Omega(0)} \left(\frac{D\rho}{Dt}\mathbf{u} + \rho\frac{D\mathbf{u}}{Dt} + \rho\mathbf{u}(\nabla\cdot\mathbf{u})\right) J\,dV_a \end{aligned}$$

$$= \int_{\Omega(0)} \rho \frac{D\mathbf{u}}{Dt} J \, dV_a = \int_{\Omega(t)} \rho \frac{D\mathbf{u}}{Dt}(\mathbf{x},t) \, dV_x. \tag{1.8}$$

According to Newton's second law, the rate of change of the momentum in the material volume $\Omega(t)$ must balance with any forces acting on the contained fluid. The forces on the fluid come in two varieties: external body forces such as gravity, which we denote as a force per unit volume by $\mathbf{f}$, and surface forces such as viscous or elastic stresses, which we denote as a force per unit area by $\mathbf{t}$, the traction. The surface of the fluid volume is described locally by the outward-pointing unit normal vector, denoted by $\mathbf{n}$, and the surface traction may be represented generally as $\mathbf{t} = \mathbf{n} \cdot \boldsymbol{\sigma}$, where $\boldsymbol{\sigma}$ is the Cauchy stress tensor (see Sect. 2.4). The standard proof of this representation is achieved by applying Newton's second law to a tetrahedron of shrinking volume (see [3]). Balancing the forces, another application of Newton's second law, now to an arbitrary material volume, provides the following integral form of momentum conservation,

$$\frac{d}{dt}\mathbf{p}(t) = \int_{\Omega(t)} \rho \frac{D\mathbf{u}}{Dt} \, dV_x = \int_{\Omega(t)} \mathbf{f} \, dV_x + \int_{\partial\Omega(t)} \mathbf{t} \, dS_x, \tag{1.9}$$

where $\partial\Omega(t)$ is the boundary of $\Omega(t)$ and dS_x is an infinitesimal surface area element. The last integral can be converted to a volume integral using the divergence theorem, so that

$$\int_{\Omega(t)} \rho \frac{D\mathbf{u}}{Dt} \, dV_x = \int_{\Omega(t)} \mathbf{f} \, dV_x + \int_{\Omega(t)} \nabla \cdot \boldsymbol{\sigma} \, dV_x. \tag{1.10}$$

Since the above holds for all material volumes, we arrive at the general differential form of momentum conservation:

$$\rho \frac{D\mathbf{u}}{Dt} = \mathbf{f} + \nabla \cdot \boldsymbol{\sigma}. \tag{1.11}$$

2.4 The Cauchy Stress Tensor and the Navier–Stokes Equations

The wide array of mathematical models for vastly different types of materials and fluids reduce to a specification of the Cauchy stress tensor, $\boldsymbol{\sigma}$. In a classical elastic solid the stress tensor depends locally on the material deformation; in a classical viscous fluid the stress tensor depends locally on the *rate* of material deformation. Generally, however, and particularly for the complex fluids to be described in this book, $\boldsymbol{\sigma}$ may even evolve in a nonlinear and history-dependent way through a partial differential equation of its own.

The components of the stress tensor may be interpreted by considering a cubic volume as illustrated in Fig. 1.2. Since the traction (the force per unit area) on a

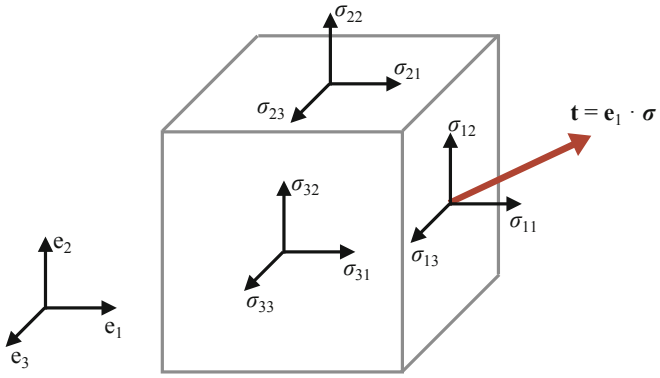

Fig. 1.2 The stress tensor $\boldsymbol{\sigma}$ contains all of the information about the surface tractions, save for the surface geometry. The traction (force per unit area) on the rightmost face of the cube, which is characterized by the outward pointing normal vector $\mathbf{e}_1$, is given by $\mathbf{t} = \mathbf{e}_1 \cdot \boldsymbol{\sigma} = \sigma_{11}\mathbf{e}_1 + \sigma_{12}\mathbf{e}_2 + \sigma_{13}\mathbf{e}_3$

surface is represented generally as $\mathbf{t} = \mathbf{n} \cdot \boldsymbol{\sigma}$, where $\mathbf{n}$ is the unit normal vector pointing out of the control volume, σ_{ij} represents the traction in the jth direction on a surface which is perpendicular to the ith direction. The traction on the rightmost boundary in Fig. 1.2, for instance, is given by $\mathbf{t} = \mathbf{e}_1 \cdot \boldsymbol{\sigma} = \sigma_{11}\mathbf{e}_1 + \sigma_{12}\mathbf{e}_2 + \sigma_{13}\mathbf{e}_3$.

The net force $\mathbf{F}$ and the torque $\mathbf{L}$ about a point $\mathbf{x}_0$ acting on an immersed body with boundary denoted by ∂S are given by integrating the traction over the surface:

$$\mathbf{F} = \int_{\partial S} \mathbf{n} \cdot \boldsymbol{\sigma}\, dS, \quad \mathbf{L} = \int_{\partial S} (\mathbf{x} - \mathbf{x}_0) \times (\mathbf{n} \cdot \boldsymbol{\sigma})\, dS. \tag{1.12}$$

In every case considered in this book, there are no body torques that may give rise to internal angular momentum. The consequence is a broad statement about the stress tensor; namely, for all materials studied in this book, the stress tensor is symmetric

$$\boldsymbol{\sigma} = \boldsymbol{\sigma}^T. \tag{1.13}$$

This result is recovered by evaluating the torque on a small control volume and imposing the conservation of angular momentum (see [3]). One important consequence of this fact is that the complete specification of the stress tensor in three dimensions requires the identification of only six components instead of nine.

The discussion thus far has made no assumptions about the specific fluid or material, and the relations above apply to any continuum model. Where the nature of the particular fluid of interest enters into the modeling is in the statement of a *constitutive law*, or a specification of the fluid response to deformation. This is

achieved by establishing an equation for the evolution of the stress tensor $\boldsymbol{\sigma}$, which is commonly written as

$$\boldsymbol{\sigma} = -p\mathbf{I} + \boldsymbol{\tau}, \tag{1.14}$$

where p is the pressure, $\mathbf{I}$ is the identity operator, and $\boldsymbol{\tau}$ is the *deviatoric stress tensor* which contains viscous and other stresses. The pressure may be of thermodynamic origin, but often is defined to represent the isotropic part of the stress tensor so as to render $\boldsymbol{\tau}$ traceless (though that is not done in much of this chapter). Many constitutive laws, including that which results in a *Newtonian* fluid model and the Navier–Stokes equations, relate the deviatoric stress to the local strain rate, which we now describe.

Consider the velocity field written in the spatial coordinates, $\mathbf{u}(\mathbf{x},t)$. Taking the convention that $(\nabla\mathbf{u})_{ij} = \partial u_j/\partial x_i$, the first terms in a Taylor expansion of the velocity field about a point $\mathbf{x}$ in space are given by

$$\mathbf{u}(\mathbf{x}+d\mathbf{x},t) = \mathbf{u}(\mathbf{x},t) + d\mathbf{x}\cdot\nabla\mathbf{u}(\mathbf{x},t) + O\left(|d\mathbf{x}|^2\right). \tag{1.15}$$

The gradient of the velocity field is usefully decomposed into its symmetric and antisymmetric parts, $\nabla\mathbf{u} = (\dot{\boldsymbol{\gamma}} + \boldsymbol{\omega})/2$, where

$$\dot{\boldsymbol{\gamma}} = \left(\nabla\mathbf{u} + (\nabla\mathbf{u})^T\right), \quad \boldsymbol{\omega} = \left(\nabla\mathbf{u} - (\nabla\mathbf{u})^T\right). \tag{1.16}$$

$\dot{\boldsymbol{\gamma}}$ is the (symmetric) rate-of-strain tensor, and $\boldsymbol{\omega}$ is the (antisymmetric) vorticity tensor. Consider a line element $d\mathbf{x}$ extending from a point $\mathbf{x}$ that evolves in a linear flow field. Then $d(d\mathbf{x})/dt = \mathbf{u}(\mathbf{x}+d\mathbf{x},t) - \mathbf{u}(\mathbf{x},t) = d\mathbf{x}\cdot(\dot{\boldsymbol{\gamma}} + \boldsymbol{\omega})/2$. Let us consider the response of the line element to the velocity gradient through the roles of the symmetric and antisymmetric parts separately. First, the action of $\dot{\boldsymbol{\gamma}}$ is best appreciated through its spectral decomposition. Since $\dot{\boldsymbol{\gamma}}$ is symmetric its eigenvectors are orthogonal, which we write as $\mathbf{d}_i$ for $i = 1,2,3$ (the *principle axes* of $\dot{\boldsymbol{\gamma}}$), and the eigenvalues $2\lambda_i$ associated with the principal axes are twice the *principal rates-of-strain*. Then we may represent the symmetric tensor $\dot{\boldsymbol{\gamma}}$ as $\sum_i (2\lambda_i)\mathbf{d}_i\mathbf{d}_i$, where $\mathbf{d}_i\mathbf{d}_i$ is a dyadic product, so if the flow gradient has only a symmetric part then

$$\frac{d}{dt}d\mathbf{x} = \frac{1}{2}d\mathbf{x}\cdot\dot{\boldsymbol{\gamma}} = \sum_i \lambda_i (d\mathbf{x}\cdot\mathbf{d}_i)\mathbf{d}_i. \tag{1.17}$$

A spherical control volume is thus instantaneously deformed by $\dot{\boldsymbol{\gamma}}$ to an ellipsoid along the principal axes of $\dot{\boldsymbol{\gamma}}$ with axis lengths indicated by the principal rates-of-strain. Meanwhile, the response of the line element $d\mathbf{x}$ to the antisymmetric part of the flow, $\boldsymbol{\omega}$, is a rigid body rotation,

$$\frac{d}{dt}d\mathbf{x} = \frac{1}{2}d\mathbf{x}\cdot\boldsymbol{\omega} = \frac{1}{2}(\nabla\times\mathbf{u})\times d\mathbf{x}, \tag{1.18}$$

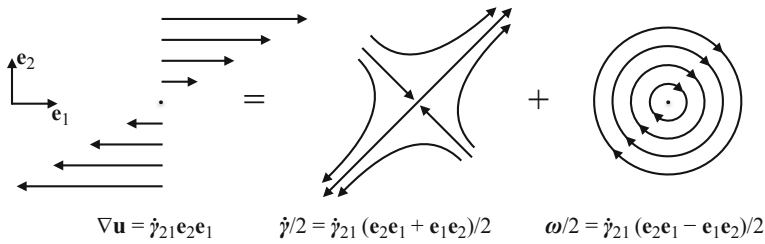

Fig. 1.3 A linear shear flow is decomposed into its extensional (symmetric) and rotational (antisymmetric) components, $\nabla\mathbf{u} = (\dot{\boldsymbol{\gamma}} + \boldsymbol{\omega})/2$

where $\nabla \times \mathbf{u}$ is the *vorticity*. An example of the decomposition of $\nabla\mathbf{u}$ into its symmetric and antisymmetric parts is shown in Fig. 1.3. A linear shear flow $\mathbf{u}(\mathbf{x},t) = \mathbf{x} \cdot (\dot{\gamma}_{21}\mathbf{e}_2\mathbf{e}_1) = (\dot{\gamma}_{21}y, 0, 0)$, where $\dot{\gamma}_{21}$ is a constant shear rate, contains both extensional (symmetric) and rotational (antisymmetric) features.

A classical (Newtonian) viscous fluid is defined to be that in which the deviatoric stress is linear in the rate of strain and the fluid is isotropic (there is no preferred direction in the fluid response to deformation). Given that the stress is symmetric, the most general form of the deviatoric stress tensor that satisfies these constraints reduces to a linear combination of $\dot{\boldsymbol{\gamma}}$ and $(\nabla \cdot \mathbf{u})\mathbf{I}$. Decomposing this general form into a traceless part and an isotropic part, the resulting constitutive relation is given by

$$\boldsymbol{\tau} = \mu \left(\dot{\boldsymbol{\gamma}} - \frac{2}{3}(\nabla \cdot \mathbf{u})\mathbf{I} \right) + \mu'(\nabla \cdot \mathbf{u})\mathbf{I}. \tag{1.19}$$

The coefficient of the traceless part of $\boldsymbol{\tau}$, or μ, is the fluid viscosity, while μ' is the dilational viscosity. In the event that the fluid is incompressible ($\nabla \cdot \mathbf{u} = 0$) then Eq. (1.19) reduces to $\boldsymbol{\tau} = \mu\dot{\boldsymbol{\gamma}}$ and the total stress tensor has the simple form

$$\boldsymbol{\sigma} = -p\mathbf{I} + \mu\dot{\boldsymbol{\gamma}}. \tag{1.20}$$

Let us now revisit the momentum balance equation. Inserting the stress above into Eq. (1.11), we obtain the equations

$$\rho \frac{D\mathbf{u}}{Dt} = -\nabla p + \mu\nabla^2\mathbf{u} + \mathbf{f}, \tag{1.21}$$

$$\nabla \cdot \mathbf{u} = 0. \tag{1.22}$$

Equations (1.21) and (1.22) are known as the incompressible Navier–Stokes equations.

2.5 Dimensional Analysis and the Stokes Equations

An important practice in the development of theory is to nondimensionalize the equations of motion, which reduces (often dramatically) the number of parameters that characterize the dynamics. Consider a flow with a characteristic time scale T, velocity scale U, and length scale L. For instance, U might be a swimming speed or a background flow speed, and L might be the approximate length of an immersed body or the gap width in a channel. Defining the dimensionless variables,

$$\mathbf{x}^* = \mathbf{x}/L, \quad \mathbf{u}^* = \mathbf{u}/U, \quad t^* = t/T, \quad p^* = Lp/(\mu U), \quad \mathbf{f}^* = L^2\mathbf{f}/(\mu U), \tag{1.23}$$

and inserting them into Eqs. (1.21) and (1.22), the dimensionless incompressible Navier–Stokes equations are obtained:

$$\mathrm{Re}\left(\mathrm{St}\frac{\partial \mathbf{u}^*}{\partial t^*} + \mathbf{u}^* \cdot \nabla \mathbf{u}^*\right) = -\nabla p^* + \nabla^2 \mathbf{u}^* + \mathbf{f}^*, \quad \nabla \cdot \mathbf{u}^* = 0. \tag{1.24}$$

Here we have introduced the dimensionless *Reynolds* and *Strouhal* numbers,

$$\mathrm{Re} = \frac{\rho U L}{\mu}, \quad \mathrm{St} = \frac{L}{UT}, \tag{1.25}$$

which characterize the flow. If the characteristic time scale is chosen to be the time for a velocity perturbation to be transported convectively by the flow, $T = L/U$, then $St = 1$. The Reynolds number indicates the relative importance of inertial effects to viscous dissipation in (1.24), and also gives the ratio between the time scale for a velocity perturbation to diffuse away due to viscosity, $\rho L^2/\mu$, and the convective time scale L/U.

The topics of interest in this book will focus on complex fluid flows at exceedingly small Reynolds numbers. For instance, in the fluid flow generated by the swimming of microorganisms, the relevant Reynolds number is on the order of 10^{-4}–10^{-2}. A common simplifying assumption is then to consider the idealized zero Reynolds number flow, resulting in the Stokes equations:

$$-\nabla p + \mu \nabla^2 \mathbf{u} + \mathbf{f} = \mathbf{0}, \quad \nabla \cdot \mathbf{u} = 0. \tag{1.26}$$

The linearity of the Stokes equations makes many methods of solution possible; in particular, Green's functions (fundamental singular solutions) may be derived and used to write representation formulae for the flow in terms of integrals over the fluid boundaries, and the Lorentz reciprocal theorem (see Chap. 8) may be used in many settings with tremendous effect. The reader is referred to [7] for a thorough discussion on the fundamental solutions and boundary-integral representations of Stokes flow and also to Chap. 11 where this approach is used in the study of blood flow.

In certain settings a more appropriate choice of characteristic time scale is related to the frequency of oscillation, ω, as may be relevant in rotational rheometers, or a frequency of undulation, as in flagellar locomotion. Taking $T = \omega^{-1}$, the Strouhal number is $St = L\omega/U$. Even for very small Reynolds numbers, $\mathrm{Re} \ll 1$, a sufficiently large frequency may result in $\mathrm{Re}\,\mathrm{St} = O(1)$, specifically, when $\rho L^2\omega/\mu = O(1)$. This ratio is commonly referred to as the frequency Reynolds number. In this setting, the time scale for viscous diffusion of a velocity perturbation, $\rho L^2/\mu$, is commensurate with the time scale of oscillation. The resulting idealized equations are the *unsteady* Stokes equations, where the momentum balance equation in (1.26) is replaced by $\rho\,\mathbf{u}_t = -\nabla p + \mu\nabla^2\mathbf{u} + \mathbf{f}$.

3 Generalized Newtonian Fluids

In the previous section we introduced the classical Newtonian constitutive model, Eq. (1.20), which is a linear relationship between the stress and velocity gradient in the fluid. This linear relationship can be viewed as the first term in a Taylor expansion of the true constitutive equation for the material in terms of small velocity gradients. The Newtonian approximation has been shown to work remarkably well for fluids consisting of small molecules, like water, liquid argon, etc., even at flow rates corresponding to fast and turbulent flows. Its success can be attributed to the separation of length and time scales in the flows of such fluids; realistic flows of Newtonian fluids do not alter the dynamics of individual constituents (atoms, molecules, etc.). In other words, typical intermolecular distances or velocity distributions of individual constituents even in very turbulent flows are the same as at rest, and, hence, the energy dissipation mechanism in the fluid, which is represented by viscosity in the Newtonian constitutive law, is not affected by the flow.

Only when the applied flows are capable of altering the local microstructure of the fluid might the classical Newtonian approximation fail to provide an adequate mathematical model of the dynamics. In Newtonian fluids this corresponds to velocity fields varying either across fluid parcels of order 10–100 particles or on time scales comparable to typical stress relaxation times. In simple fluids like liquid argon, the stress relaxation time scale is related to the typical time of molecular self-diffusion and is on the order of 10^{-13}–10^{-12} s [8]. Accessing either of these regimes requires very large velocity gradients that are very rarely achieved in natural or even experimental environments.

The situation is very different for solutions of colloidal particles, long flexible polymers, wormlike micelles, and similar *complex* fluids [9]. These particles are significantly larger than individual molecules of typical Newtonian fluids discussed above, and the time scales of stress relaxation in complex fluids are significantly longer than in their Newtonian counterparts and can easily be achieved in real-life situations. For example, in colloidal suspensions, while in dilute polymer solutions

the stress relaxation time is proportional to the time required for a single polymer to regain its equilibrium configuration after being stretched, the Maxwell relaxation time, and is typically of order 10^{-3}–10^{0} s [9]. Although there are often multiple mechanisms of stress relaxation in complex fluids, one can use the longest relaxation time λ to form a dimensionless group $\mathrm{Wi} = \lambda\dot{\gamma}$—the Weissenberg number. Here, the shear rate $\dot{\gamma} = \sqrt{(\dot{\boldsymbol{\gamma}} : \dot{\boldsymbol{\gamma}})/2}$ is an invariant measure of the rate of strain in the fluid (see Sect. 3.1). For small velocity gradients, $\mathrm{Wi} \ll 1$, complex fluids obey the linear constitutive law, Eq. (1.20), and flow like Newtonian fluids at the same Reynolds number. When the Weissenberg number is comparable to or larger than unity, complex fluids exhibit non-Newtonian behavior and obey complicated constitutive models, often involving nonlinear dependence of the local stress on the velocity gradient and the deformation history of the fluid. In this section we focus on the simplest extension of Eq. (1.20) in which the flow only influences the instantaneous viscosity of the fluid, the so-called *generalized Newtonian model*. A general theory dealing with history-dependent properties of viscoelastic fluids will be discussed in the following sections.

3.1 Shear-Thinning and Shear-Thickening Fluids

A generalized Newtonian fluid is a phenomenological model that assumes that the applied flow only changes the dissipation rate in the fluid (i.e., its viscosity), but does not change the tensorial structure of the Newtonian constitutive model Eq. (1.20). The constitutive laws for this class of models can be written in the following general form:

$$\boldsymbol{\sigma} = -p\mathbf{I} + \eta(\dot{\boldsymbol{\gamma}})\dot{\boldsymbol{\gamma}}, \tag{1.27}$$

where $\eta(\dot{\boldsymbol{\gamma}})$ is the viscosity, made distinct from the Newtonian viscosity μ due to its possible dependence upon the fluid flow. First note that the local viscosity η can only depend on the invariants of the tensor $\dot{\boldsymbol{\gamma}}$, otherwise a similarity transform (a change of coordinate system) could change the value of the viscosity, which is unphysical. Also, it would be natural to require in the linear shear flow with a constant shear rate $\dot{\gamma}_{21}$ considered in the previous section, $\mathbf{u}(\mathbf{x},t) = (\dot{\gamma}_{21}y, 0, 0)$, that the viscosity should simply be a function of the scalar $\dot{\gamma}_{21}$. The second tensorial invariant of $\dot{\boldsymbol{\gamma}}$ is the lowest invariant that satisfies this condition, and we may write

$$\eta(\dot{\boldsymbol{\gamma}}) = \eta(\dot{\gamma}), \tag{1.28}$$

where

$$\dot{\gamma}^2 = \frac{1}{2}\dot{\boldsymbol{\gamma}} : \dot{\boldsymbol{\gamma}} = \frac{1}{2}(\nabla\mathbf{u} + \nabla\mathbf{u}^T)_{ij}(\nabla\mathbf{u} + \nabla\mathbf{u}^T)_{ji}, \tag{1.29}$$

summing over both repeated indices. The material properties of a generalized Newtonian fluid are determined entirely by the behavior of the function $\eta(\dot{\gamma})$. The simplest possibility, a monotonic function, results in:

- $\partial\eta/\partial\dot{\gamma} > 0$, a *shear-thickening* fluid, or
- $\partial\eta/\partial\dot{\gamma} < 0$, a *shear-thinning* fluid.

Shear-thickening fluids, as the name suggests, exhibit an increasing resistance to shear as the shear rate increases, while shear-thinning fluids exhibit the opposite behavior; "Oobleck" (cornstarch and water) and pastes are typical examples of the former type of fluids, while solution and melts of long flexible polymers and semidilute solutions of wormlike micelles are examples of the latter. Real materials can exhibit complicated combinations of the two, e.g., shear-thinning at low shear rates followed by shear-thickening at higher shear rates [10]. While these trends can easily be incorporated into a model for $\eta(\dot{\gamma})$, the generalized constitutive law, Eq. (1.27), is a strictly phenomenological model that mimics all the changes in the internal structure of the fluid due to the applied flow by a shear-dependent effective viscosity. The presence of shear-thinning and shear-thickening in the same material typically implies several competing mechanisms of stress creation and relaxation, and a naive model like Eq. (1.27) would most certainly fail in properly describing even simple flows of such fluids. Therefore, generalized Newtonian models should only be used in flows of complex fluids where there is a good reason to believe that the dynamics of principle concern are caused by the shear-induced changes in the viscosity of the fluid and only in the simplest of flows.

3.2 Carreau–Yasuda and Power-Law Fluids

One of the most popular models for shear-thinning fluids is the Carreau–Yasuda viscosity model:

$$\eta(\dot{\gamma}) = \eta_\infty + (\eta_0 - \eta_\infty)\left[1 + \left(\lambda\dot{\gamma}\right)^a\right]^{\frac{n-1}{a}} \qquad \textit{(Carreau–Yasuda)} \tag{1.30}$$

that interpolates between the *zero-shear-rate viscosity* η_0 and the *infinite-shear rate viscosity* η_∞. A relaxation time λ sets the crossover shear rate: for $\dot{\gamma} < \lambda^{-1}$, the Carreau–Yasuda fluid exhibits, essentially, a Newtonian behavior with the viscosity η_0, while for higher shear rates its viscosity drops to $\eta_\infty < \eta_0$. The Carreau–Yasuda model contains two constants: the power-law index $n < 1$ that characterizes the degree of shear-thinning of the model and the constant a that sets the size and curvature of the crossover region between the Newtonian and shear-thinning behavior. A typical viscosity of the Carreau–Yasuda model is shown in Fig. 1.4.

For high shear rates, $\lambda\dot{\gamma} \gg 1$, the Carreau–Yasuda model can be simplified significantly to

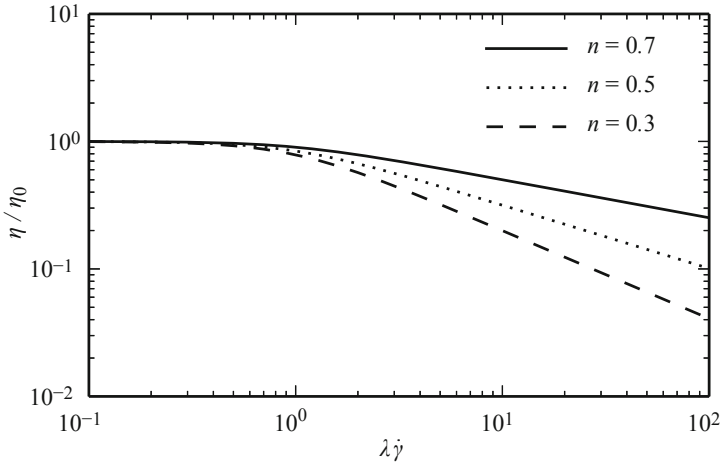

Fig. 1.4 Viscosity of the Carreau–Yasuda model for various values of the power index n with $\eta_\infty/\eta_0 = 10^{-3}$ and $a = 2$

$$\eta(\dot{\gamma}) \approx \eta_\infty + (\eta_0 - \eta_\infty)\left(\lambda\dot{\gamma}\right)^{n-1}. \tag{1.31}$$

The second term in this expression corresponds to the *power-law* model, which is closely related to the Carreau–Yasuda model, Eq. (1.30). To reduce the number of parameters, it is customary to write this term as $K\dot{\gamma}^{n-1}$, although the parameter K in this expression has the strange dimensions of Pa·s^n. Since the constitutive law corresponding to Eq. (1.31) is a sum of two contributions, a Newtonian term with the viscosity η_∞ and a power-law term, one can study the latter separately. Also, the relative magnitude of the Newtonian term in Eq. (1.31) is typically much smaller than the power-law contribution and can safely be neglected. This is the case, for example, in dilute polymer solutions where the Newtonian contribution in Eq. (1.31) corresponds to the viscosity of the solvent η_∞, while at moderate shear rates, the viscosity of the solution, $\eta_\infty + (\eta_0 - \eta_\infty)(\lambda\dot{\gamma})^{n-1}$, is typically several orders of magnitude larger.

In order to illustrate the typical features of flows of shear-thinning materials, we now consider flow in a pipe of a power-law fluid. We choose the cylindrical coordinate system with the z-direction along the axis of the pipe of radius R. The flow is assumed to be laminar, unidirectional, and axisymmetric, $\mathbf{u} = (0, 0, U(r))$, and the second tensorial invariant of $\dot{\boldsymbol{\gamma}}$ reduces to $\dot{\gamma} = |U'(r)|$, where the prime denotes the r-derivative. Combining the momentum balance equation (1.11), the generalized Newtonian constitutive law, Eq. (1.27), and the power-law model for the viscosity, $\eta(\dot{\gamma}) = K\dot{\gamma}^{n-1}$, we obtain the following equation of motion:

$$-\partial_z p + \frac{1}{r}\partial_r(r\sigma_{rz}) = 0, \tag{1.32}$$

where the shear stress σ_{rz} is given by

$$\sigma_{rz} = K U'(r) \left| U'(r) \right|^{n-1}. \tag{1.33}$$

The flow is driven by the applied constant pressure gradient $-\partial_z p = \Delta P/L = (P_{\text{inlet}} - P_{\text{outlet}})/L$, where L is the pipe length. Integrating Eq. (1.32) and requiring that the shear stress remains finite on the centerline $r = 0$, we obtain the following distribution of the shear stress in the cross section of the pipe

$$\sigma_{rz}(r) = -\sigma_w \frac{r}{R}, \tag{1.34}$$

where

$$\sigma_w = \frac{1}{2} \frac{\Delta P}{L} R \tag{1.35}$$

is the value of the shear stress at the wall. At the wall, we expect the fluid to satisfy the no-slip boundary condition, $U(R) = 0$, and therefore $U'(r)$ should be negative resulting in the following equation for the velocity:

$$K \left| U'(r) \right|^n = \sigma_w \frac{r}{R}. \tag{1.36}$$

Integrating this equation with the no-slip boundary condition, we obtain

$$U(r) = \left(\frac{\sigma_w}{K} \right)^{\frac{1}{n}} \frac{nR}{n+1} \left[1 - \left(\frac{r}{R} \right)^{\frac{n+1}{n}} \right]. \tag{1.37}$$

For the Newtonian case, $n = 1$, we have $K = \mu$, the Newtonian viscosity, and Eq. (1.37) reduces to the usual parabolic Hagen–Poiseuille profile:

$$U(r) = \frac{\Delta P R^2}{4 L \mu} \left[1 - \left(\frac{r}{R} \right)^2 \right]. \tag{1.38}$$

To demonstrate the effect of shear-thinning on the spatial profile in the pipe, we normalize Eq. (1.37) with the mean velocity in the pipe

$$\overline{U} = \frac{1}{\pi R^2} \int_0^{2\pi} d\theta \int_0^R U(r)\, r\, dr = \left(\frac{\sigma_w}{K} \right)^{\frac{1}{n}} \frac{nR}{3n+1}, \tag{1.39}$$

to obtain

$$\frac{U(r)}{\overline{U}} = \frac{3n+1}{n+1} \left[1 - \left(\frac{r}{R} \right)^{\frac{n+1}{n}} \right]. \tag{1.40}$$

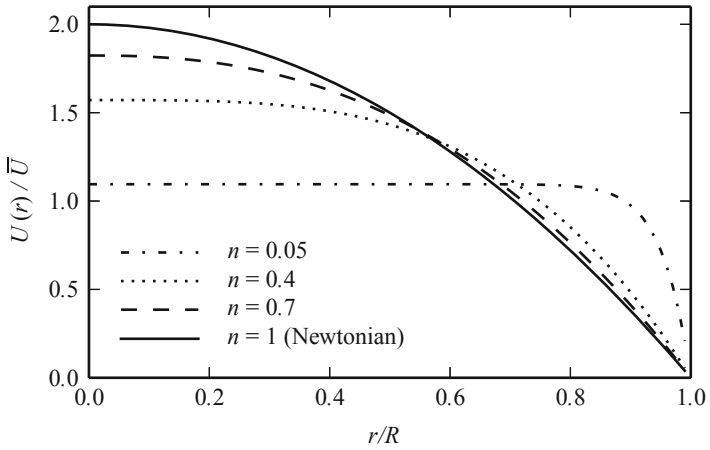

Fig. 1.5 The normalized velocity profile of a pressure-driven pipe flow, from Eq. (1.40), for various values of the power-law index n. As the fluid becomes more shear-thinning (decreasing n), the high-shear region of the flow moves progressively towards the wall and the region near the center of the pipe becomes more plug-like

The normalized velocity profile, Eq. (1.40), is shown in Fig. 1.5 for various values of the power-law index n. As the fluid becomes more shear-thinning (decreasing n), the high-shear region of the flow moves progressively towards the wall and the region near the center of the pipe becomes more plug-like. This is typical of all shear flows of shear-thinning fluids: they split into regions with high shear rates near boundaries where the local viscosity of the fluid is low and parts that move almost like solid bodies. As Eq. (1.40) suggests, in the pipe flow the tendency for shear to localize next to a boundary increases as n decreases until n reaches zero, at which point Eq. (1.40) becomes unphysical. This is a signal of a more general mechanical instability present in shear flows of extremely shear-thinning fluids, to which we now turn.

3.3 Mechanical Instability of Extremely Shear-Thinning Fluids

To demonstrate the origin of the mechanical instability mentioned above, we consider a plane Couette flow (linear shear flow) of a shear-thinning fluid. The fluid is confined between two parallel plates located at $y = 0$ and $y = h$ in a 2-dimensional Cartesian coordinate system $\mathbf{x} = (x, y)$. The base flow is given by $\mathbf{u}(\mathbf{x}) = (\dot{\gamma}_0 y, 0) = (u(y), 0)$, and the equations of motion and the constitutive equation are given by Eqs. (1.11) and (1.27). The upper wall moves with the velocity $\dot{\gamma}_0 h$ in its plane while the lower wall is kept stationary.

Consider an infinitesimal perturbation to the base profile of the following form:

$$\mathbf{u}(\mathbf{x},t) = (\dot{\gamma}_0 y, 0) + (\delta u(y,t), 0)\,. \tag{1.41}$$

This perturbation deforms the original profile but does not change the unidirectional nature of the flow. An equation of motion for the perturbation reduces to

$$\rho \frac{\partial}{\partial t}\delta u(y,t) = \frac{\partial}{\partial y}\left\{\left(\dot{\gamma}_0 + \frac{\partial}{\partial y}\delta u(y,t)\right)\eta\left(\dot{\gamma}_0 + \frac{\partial}{\partial y}\delta u(y,t)\right)\right\}. \tag{1.42}$$

Assuming the perturbation to be small relative to the background shear flow, a linearization of this equation returns:

$$\rho \frac{\partial}{\partial t}\delta u(y,t) = \left(\eta(\dot{\gamma}_0) + \dot{\gamma}_0 \frac{\partial \eta}{\partial \dot{\gamma}}(\dot{\gamma}_0)\right)\frac{\partial^2}{\partial y^2}\delta u(y,t). \tag{1.43}$$

The no-slip boundary conditions are already satisfied by the base profile, so that the perturbation must have $\delta u(0,t) = \delta u(h,t) = 0$. Therefore, without loss of generality, the perturbation can be written as

$$\delta u(y,t) = \sum_{m=1}^{\infty} \delta u_m e^{\alpha_m t} \sin\frac{m\pi y}{h}. \tag{1.44}$$

Here the δu_m are unknown coefficients of the expansion and α_m is an eigenvalue associated with the Fourier mode m. If the real part of α_m is positive, the corresponding Fourier mode will grow exponentially in time, indicating a loss of stability of the base flow. Substituting this expansion into the equation of motion we obtain

$$\alpha_m = -\left(\frac{m\pi}{h}\right)^2\left(\eta(\dot{\gamma}_0) + \dot{\gamma}_0\frac{\partial\eta}{\partial\dot{\gamma}}(\dot{\gamma}_0)\right). \tag{1.45}$$

For a power-law fluid, $\eta(\dot{\gamma}) = K\dot{\gamma}^{n-1}$, the term in parentheses reduces to $nK\dot{\gamma}_0^{n-1}$, and hence α_m is positive for $n < 0$. In other words, steady shear flows of shear-thinning fluids with a power-law steeper than -1 are unstable and cannot be realized. More generally, Eq. (1.45) implies that any shear flow is unstable if its shear stress σ_{12} decreases with $\dot{\gamma}$, i.e.,

$$\frac{\partial\sigma_{12}}{\partial\dot{\gamma}} < 0. \tag{1.46}$$

Generally, in dilute polymer solutions this condition is never satisfied and steady shear flows are possible for these fluids. However, linear shear flows of semidilute wormlike micellar solutions have been demonstrated to split into piecewise linear

shear flow with regions of different shear rates. This phenomenon of *shear-banding* is well studied and is usually attributed to the region of the flow where Eq. (1.46) is satisfied. Comprehensive reviews of shear-banding can be found elsewhere [11, 12].

4 Differential Constitutive Equations for Viscoelastic Fluids

In the previous section we introduced the generalized Newtonian fluid model, a simple extension of the linear relation between the stress and velocity gradient in the classical Newtonian constitutive law. While exhibiting shear-dependent viscosity these fluids are essentially Newtonian in the following aspects: the structure of the stress tensor of generalized Newtonian fluids in a particular flow is the same as in their Newtonian counterparts, and their velocity fields adjust instantaneously to changes in stresses. Many complex fluids behave quite differently. One of the key features of viscoelastic fluids is the presence of memory; stresses in such fluids depend on the flow history. Another is stress anisotropy. Generally, a viscoelastic fluid generates stresses that are absent in a Newtonian fluid subjected to the same deformation history.

The consequences of these features are dramatic: viscoelastic fluids do not flow like their Newtonian counterparts. In this section, we develop a mathematical framework that will allow us to incorporate memory and stress anisotropy into constitutive equations for viscoelastic fluids. Unfortunately, there is no single model that describes all viscoelastic fluids similar to the Navier–Stokes equations for Newtonian flows. Instead, one usually chooses a model that is known to describe a particular type of fluid microstructure in a particular type of flow. In this section we introduce several popular models used for polymer solutions and discuss their physical interpretations and the domains of their applicability.

4.1 Linear Maxwell Fluids and Kelvin–Voigt Solids

Viscoelastic fluids are materials that exhibit both viscous and elastic responses to forces. The distinction between viscous and elastic materials is best illustrated by their responses to a sudden deformation: stresses created in an elastic material stay constant in time for as long as the deformation is present, while stresses in a viscous fluid dissipate on a time scale governed by its viscosity. For example, a bow is stressed as long as it is strung by a bowstring, while in spilled water all stresses disappear once the fluid comes to rest. Essentially, whether a material is fluid-like or solid-like is determined by its longtime response to a deformation.

To explore the distinction between the two types of responses, consider a simple shear deformation where adjacent layers of a material are shifted impulsively in the same direction along their planes relative to each other. The strength of this deformation can be characterized by its gradient, denoted by γ, which for small

Fig. 1.6 Graphical depiction of two types of material response: (*left*) a dashpot (viscous fluid) and (*right*) a spring (elastic solid)

Fig. 1.7 Illustrations of the one-dimensional (*left*) Maxwell and (*right*) Kelvin–Voigt linear viscoelastic models

displacements is approximated as the ratio of the total relative shift between two layers to the distance between them. The shear stress σ created in an elastic solid by such a deformation obeys Hooke's law and can be written as

$$\sigma = G\gamma, \tag{1.47}$$

where G is the elastic constant of the material, or *shear modulus*. Meanwhile, the constitutive equation for a Newtonian viscous fluid is a linear relationship between the stress and velocity gradient, Eq. (1.20), and, adopted to the case of present interest, reads

$$\sigma = \eta\,\dot{\gamma}. \tag{1.48}$$

Here, as before, η is the viscosity of the fluid, and the dot denotes a time derivative. Note the distinction between $\dot{\gamma}$, the velocity gradient, and γ, the displacement gradient. Due to obvious similarities, linear solids and liquids are often denoted graphically by springs and dashpots (shock-absorbing devices based on viscous fluids used, for example, to prevent doors from slamming); see Fig. 1.6. The simplest viscoelastic material is a linear combination of the two types of material responses discussed above. In direct analogy with electric circuits, one can think of either *serial* or *parallel* connection between the basic elements from Fig. 1.6, and the two possible combinations are shown in Fig. 1.7. Each combination should be thought of as a fluid with both elastic and viscous properties.

The serial connection of a spring and a dashpot is a viscoelastic fluid, while the parallel connection is a viscoelastic solid. To demonstrate this we consider both types of viscoelastic elements subjected to a fixed displacements of their ends. In the serial connection, both the spring and the dashpot are stretched initially. However, the displacement of the spring can be redistributed to the dashpot, keeping the total displacement constant, and resulting in the absence of stress in this material at long

times, since $\sigma \sim \dot{\gamma}$ for a dashpot. On the contrary, the parallel connection remains under stress for as long as $\gamma \neq 0$, as evident from Fig. 1.7. Historically, these models have been called the *Maxwell fluid* and *Kelvin–Voigt solid* models, and they are the simplest models of viscoelastic materials. Alternatively, the same models are sometimes referred to as *solid-like liquids* and *liquid-like solids*, where the last word of the name identifies the model's behavior at long times.

To derive constitutive equations for the Maxwell and Kelvin–Voigt materials, we introduce the total deformation γ and the total stress σ for each model. The corresponding deformations and stresses of the spring and dashpot are denoted by γ_s and γ_d, and σ_s and σ_d, correspondingly. We note here that only the total deformation and stress are measurable quantities, while the deformations and stresses of the springs and dashpots are auxiliary variables that are used to describe internal mechanisms of stress creation and dissipation within each material. The present goal is to find a constitutive relation between σ and γ for both models. Continuing the analogy with electric circuits, we observe that $\gamma = \gamma_s + \gamma_d$ and $\sigma = \sigma_s = \sigma_d$ for the Maxwell fluid, while $\gamma = \gamma_s = \gamma_d$ and $\sigma = \sigma_s + \sigma_d$ for the Kelvin–Voigt solid. Using Eqs. (1.47) and (1.48), we obtain

$$\sigma + \frac{\eta}{G}\dot{\sigma} = \eta\,\dot{\gamma} \qquad \textit{(Maxwell fluid)}, \tag{1.49}$$

$$\sigma = G\gamma + \eta\,\dot{\gamma} \qquad \textit{(Kelvin–Voigt solid)}. \tag{1.50}$$

While neither the Kelvin–Voigt or Maxwell linear models are generally adequate for describing real materials, they are prototype models for systems like polymer brushes grafted on a surface and dilute polymer solutions, respectively. Since the scope of this chapter is complex fluids, we focus our attention on the Maxwell model.

The Maxwell model, Eq. (1.49), can be formally solved to yield

$$\sigma(t) = \frac{1}{\lambda}\int_{-\infty}^{t} e^{-\frac{t-t'}{\lambda}}\,\eta\,\dot{\gamma}(t')\,dt', \tag{1.51}$$

where we have introduced the Maxwell relaxation time $\lambda = \eta/G$. As can be seen from the solution, the stress created by a steplike deformation relaxes exponentially on the time scale λ indicating viscous-fluid-like properties, while at short times, $\sigma(t) \sim \eta\gamma(t)/\lambda$ and the Maxwell material is solid-like.

Since Eq. (1.49) is linear, its behavior is easily analyzed in terms of its response to a periodic deformation with a frequency ω. Time evolution of the stress for arbitrary time-dependent deformations may then be reconstructed through the evolution of decoupled Fourier coefficients. Integrating Eq. (1.51) with only one frequency of deformation, $\gamma(t) = \gamma_0 \sin\omega t$, we obtain

$$\sigma(t) = \gamma_0\eta\omega\frac{\cos\omega t + \lambda\omega\sin\omega t}{1+(\lambda\omega)^2} = \frac{\eta}{1+(\lambda\omega)^2}\dot{\gamma}(t) + G\frac{(\lambda\omega)^2}{1+(\lambda\omega)^2}\gamma(t). \tag{1.52}$$

Equation (1.52) demonstrates that the Maxwell model exhibits stress response both in and out of phase with the applied deformation. Comparing this expression to Eqs. (1.47) and (1.48), we conclude that the stress response can be interpreted in terms of a frequency-dependent viscosity, $\tilde{\eta}(\omega)$, and shear modulus, $\tilde{G}(\omega)$, where

$$\tilde{\eta}(\omega) = \frac{\eta}{1+(\lambda\omega)^2}, \qquad \tilde{G}(\omega) = G\frac{(\lambda\omega)^2}{1+(\lambda\omega)^2}. \tag{1.53}$$

Once again, at short times ($\lambda\omega \gg 1$), the Maxwell model behaves like a solid with the shear modulus $\tilde{G}(\omega) \approx G$, while at long times ($\lambda\omega \ll 1$) it behaves as a viscous fluid with the viscosity $\tilde{\eta}(\omega) \approx \eta$. The crossover between the two regimes occurs when the time scale of deformation is similar to the time scale of relaxation, $\omega^{-1} \sim \lambda$.

Equations (1.52) and (1.53) form the theoretical basis of linear rheology. For very small deformation amplitudes γ_0, even very nonlinear viscoelastic materials are expected to obey Eq. (1.49), and measuring the in- and out-of-phase response of the shear stress $\sigma(t)$ allows one to determine the viscosity, elastic modulus, and Maxwell relaxation time of the fluid. Linear rheological measurements are usually interpreted in terms of the complex modulus, $G^*(\omega) = G'(\omega) + iG''(\omega)$, defined for the case considered here by $\sigma(t) = \Im\left(G^*(\omega)\gamma_0 e^{i\omega t}\right)$, where $\Im(\cdot)$ denotes the imaginary part of its complex argument. Commercial rheometers readily provide the storage and loss moduli $G'(\omega)$ and $G''(\omega)$ as functions of ω (the so-called frequency sweep), and for the Maxwell model the relaxation time can be determined as $\lambda = \omega_0^{-1}$, with ω_0 as the frequency where $G'(\omega_0) = G''(\omega_0)$. The other parameters are then determined by fitting the low-frequency behaviors of G' and G''. In reality, however, the Maxwell model is often insufficient to describe even the linear rheology of polymer solutions and G' and G'' do not cross due to additional dissipation mechanisms that will be discussed later in this section. Nevertheless, it is a very useful minimal model that sets the stage for more complete theories.

4.2 Objectivity and Convected Derivatives

In Sect. 4.1 we introduced the linear Maxwell model that combines viscous and elastic responses to deformations. For the simplest case of linear shear that model was written as $\sigma + \lambda\dot{\sigma} = \eta\dot{\gamma}$, where σ is the shear stress and $\dot{\gamma}$ is the shear rate. To generalize this model for arbitrary flows, it would seem that one would only need to rewrite this equation in terms of the stress $\boldsymbol{\sigma}$ and velocity gradient $\nabla\mathbf{u}$ tensors as

$$\boldsymbol{\sigma} + \lambda\frac{\partial\boldsymbol{\sigma}}{\partial t} = \eta\dot{\boldsymbol{\gamma}}. \tag{1.54}$$

However, this equation suffers from a serious physical problem: it is not frame-invariant. To demonstrate this, assume that we perform the same experiment twice:

once in a stationary lab frame, the other on a (very smoothly operated) train moving with a constant velocity $\mathbf{u}_0$ with respect to the lab frame. The stress components of the moving-frame experiment can be written in terms of the lab frame coordinates as $\sigma_{ij}(\mathbf{x}+\mathbf{u}_0 t, t)$ and their time derivatives become

$$\frac{\partial}{\partial t}\sigma_{ij}(\mathbf{x}+\mathbf{u}_0 t, t) = \frac{\partial \sigma_{ij}}{\partial t} + \mathbf{u}_0 \cdot \nabla \sigma_{ij}. \tag{1.55}$$

Obviously, both experiments should be described by the same equations since a constant velocity added to each point in the fluid does not result in any velocity gradients; hence no additional stresses should be created in the fluid. However, the time derivatives in Eqs. (1.54) and (1.55) differ by a term proportional to $\mathbf{u}_0$. Clearly, this indicates that Eq. (1.54) is not frame-invariant and *it should not be used*.

The problem, as we can see from this example, is that the time derivatives of individual components of the stress tensor do not form a tensor themselves, i.e., the generalization $\partial\sigma/\partial t \to \partial\boldsymbol{\sigma}/\partial t$ is unphysical since it does not lead to a frame-invariant equation. This problem is reminiscent of the argument that led to the introduction of the material derivative in Eq. (1.2). There we showed that the frame-invariant time derivative of a vector field embedded in a moving fluid is given by D/Dt. Our goal now is to derive a similar expression for a second-rank tensor. A detailed treatment of this derivation can be found in [13–15].

Recall the reference and current configurations described in Sect. 2.1, illustrated again in Fig. 1.8. We will make use of the curvilinear coordinate system defined by the material (Lagrangian) coordinates, $Oa^1a^2a^3$, which moves and deforms with the fluid (the so-called *convected* frame). The new coordinates are related to the fixed Cartesian system $Ox_1x_2x_3$ by $\mathbf{x} = \mathbf{x}(\mathbf{a}, t)$, and the relation is assumed to be invertible. Recall the choice (without loss of generality) to set $\mathbf{x}(\mathbf{a}, 0) = \mathbf{a}$, so that the convected and Cartesian frames are in alignment at $t = 0$; while this is a useful illustration for how the convected frame moves and deforms, we will only make use of the convected and Cartesian frames in the current configuration.

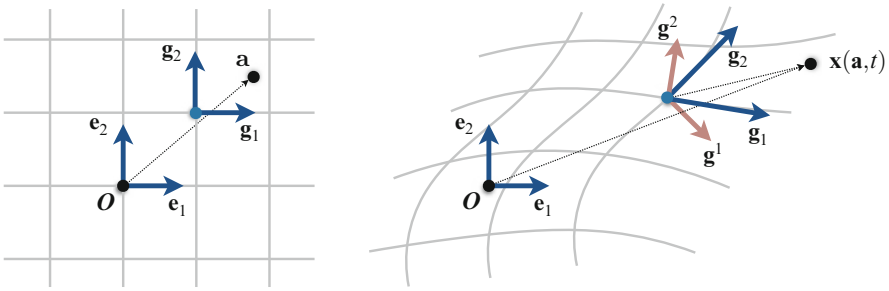

Fig. 1.8 The curvilinear, *convected* frame, has base vectors $\{\mathbf{g}_i\}$ which move and deform with the material deformation. The base vectors are aligned with the Cartesian basis $\{\mathbf{e}_i\}$ in the reference configuration (*left*). The reciprocal vectors $\{\mathbf{g}^i\}$ form an orthonormal basis and satisfy $\mathbf{g}^i \cdot \mathbf{g}_j = \delta_{ij}$. While a useful illustration, the curvilinear and Cartesian frames are only used in the current configuration (*right*) to derive objective time derivatives

Consider an arbitrary point in space, $\mathbf{x}$, which may be represented in terms of base vectors in a given, fixed curvilinear coordinate system, $\{\mathbf{g}_i\}$, as

$$\mathbf{x} = \sum_{i=1}^{3} a^i \mathbf{g}_i. \tag{1.56}$$

The base vectors may then be defined as

$$\mathbf{g}_i = \frac{\partial \mathbf{x}}{\partial a^i}, \tag{1.57}$$

which change both in length and orientation along with the material and are tangential to the lines of constant material coordinates as can be seen from their definition. In a curvilinear system we may also introduce reciprocal vectors, $\{\mathbf{g}^i\}$, that are orthogonal to the base vectors, $\{\mathbf{g}_i\}$, in the following sense: $\mathbf{g}^i \cdot \mathbf{g}_j = \delta_{ij}$, where δ_{ij} is the Kronecker delta. This implies that the reciprocal vectors are orthogonal to planes spanned by two base vectors. They can be constructed, for example, by the usual orthogonalization procedure: $\mathbf{g}^i = \mathbf{g}_j \times \mathbf{g}_k / (\mathbf{g}_i \cdot (\mathbf{g}_j \times \mathbf{g}_k))$ for all cyclic permutations of $(i,j,k) = (1,2,3)$ compatible with the right-handed coordinate system, and $\mathbf{g}_i \cdot (\mathbf{g}_j \times \mathbf{g}_k) = 1$ in an incompressible flow. Here we choose the reciprocal vectors

$$\mathbf{g}^i = \frac{\partial a^i}{\partial \mathbf{x}}, \tag{1.58}$$

which satisfy all the requirements listed above.

Observe that any point $\mathbf{x}$ may be expressed in terms of the Cartesian system, $\mathbf{x} = \sum_{j=1}^{3} x_j \mathbf{e}_j$ (see Fig. 1.8), so that

$$\mathbf{g}_i = \frac{\partial \mathbf{x}}{\partial a^i} = \frac{\partial}{\partial a^i} \sum_{j=1}^{3} x_j \mathbf{e}_j = \sum_{j=1}^{3} F_{ji} \mathbf{e}_j, \tag{1.59}$$

where

$$\mathbf{F} = \frac{\partial \mathbf{x}}{\partial \mathbf{a}} = \sum_{i,j=1}^{3} \frac{\partial x_i}{\partial a^j} \mathbf{e}_i \mathbf{e}_j \tag{1.60}$$

is the deformation gradient tensor introduced in Sect. 2.1. In a similar fashion, we may write

$$\mathbf{g}^i = \frac{\partial a^i}{\partial \mathbf{x}} = \sum_{j=1}^{3} \left(\mathbf{e}_j \frac{\partial}{\partial x_j} \right) a^i = \sum_{j=1}^{3} (F^{-1})_{ij} \mathbf{e}_j, \tag{1.61}$$

where

$$\mathbf{F}^{-1} = \frac{\partial \mathbf{a}}{\partial \mathbf{x}} = \sum_{i,j=1}^{3} \frac{\partial a^i}{\partial x_j} \mathbf{e}_i \mathbf{e}_j. \tag{1.62}$$

The deformation gradient tensors, $\mathbf{F}$ and $\mathbf{F}^{-1}$, are both expressed in terms of the fixed Cartesian basis, and naturally $\mathbf{F}^{-1} \cdot \mathbf{F} = \mathbf{F} \cdot \mathbf{F}^{-1} = \mathbf{I}$.

Next we show how $\mathbf{F}$ and $\mathbf{F}^{-1}$ change in time. Consider the time derivative of $\mathbf{F}$,

$$\frac{d}{dt} F_{ij} = \frac{d}{dt} \frac{\partial x_i}{\partial a^j} = \frac{\partial u_i}{\partial a^j} = \sum_{k=1}^{3} \frac{\partial u_i}{\partial x_k} \frac{\partial x_k}{\partial a^j} = \left[(\nabla \mathbf{u})^T \cdot \mathbf{F} \right]_{ij}, \tag{1.63}$$

or $d\mathbf{F}/dt = (\nabla \mathbf{u})^T \cdot \mathbf{F}$. The time evolution of $\mathbf{F}^{-1}$ can be obtained by taking the time derivative of the orthogonality condition, $\mathbf{F} \cdot \mathbf{F}^{-1} = \mathbf{I}$, which gives

$$\frac{d\mathbf{F}}{dt} \cdot \mathbf{F}^{-1} + \mathbf{F} \cdot \frac{d\mathbf{F}^{-1}}{dt} = 0. \tag{1.64}$$

Using $d\mathbf{F}/dt = (\nabla \mathbf{u})^T \cdot \mathbf{F}$, we obtain

$$\frac{d\mathbf{F}^{-1}}{dt} = -\mathbf{F}^{-1} \cdot (\nabla \mathbf{u})^T. \tag{1.65}$$

We are now set to derive the frame-invariant time derivative of the stress tensor or any other second-rank tensor embedded in a moving fluid. The total stress tensor $\boldsymbol{\sigma}$ may be represented alternately in terms of its Cartesian, covariant, or contravariant components:

$$\boldsymbol{\sigma} = \sum_{m,n=1}^{3} \sigma_{mn} \mathbf{e}_m \mathbf{e}_n = \sum_{i,j=1}^{3} \hat{\sigma}^{ij} \mathbf{g}_i \mathbf{g}_j = \sum_{i,j=1}^{3} \hat{\sigma}_{ij} \mathbf{g}^i \mathbf{g}^j. \tag{1.66}$$

Since the base vectors $\mathbf{g}_i$ and the reciprocal vectors $\mathbf{g}^i$ can be expressed in terms of Cartesian unit vectors, Eqs. (1.59) and (1.61), the co- and contravariant components of $\boldsymbol{\sigma}$ can be expressed through its Cartesian components as

$$\sigma_{mn} = \sum_{i,j=1}^{3} \hat{\sigma}^{ij} F_{mi} F_{nj} = \sum_{i,j=1}^{3} \hat{\sigma}_{ij} F^{-1}_{im} F^{-1}_{jn}. \tag{1.67}$$

These relations can be inverted to read

$$\hat{\sigma}^{ij} = \sum_{m,n=1}^{3} F^{-1}_{im} F^{-1}_{jn} \sigma_{mn} = [\mathbf{F}^{-1} \cdot \boldsymbol{\sigma} \cdot \mathbf{F}^{-T}]_{ij}, \tag{1.68}$$

$$\hat{\sigma}_{ij} = \sum_{m,n=1}^{3} F_{mi} F_{nj} \sigma_{mn} = [\mathbf{F}^T \cdot \boldsymbol{\sigma} \cdot \mathbf{F}]_{ij}, \tag{1.69}$$

where $\mathbf{F}^{-T} = (\mathbf{F}^{-1})^T$, and the subscripts on the right-hand side indicate components in the Cartesian coordinate system. We notice that these equations are, in fact, definitions of co- and contravariant components of a second-rank tensor, as they state the transformation laws for the components upon a change of the coordinate system. Any set of quantities that obey these transformation laws form a second-rank tensor and are thus frame-invariant.

Let us now calculate the time derivative of the co- and contravariant components of the stress tensor $\boldsymbol{\sigma}$. From Eq. (1.68),

$$\frac{d\hat{\sigma}^{ij}}{dt} = \left[\frac{d\mathbf{F}^{-1}}{dt} \cdot \boldsymbol{\sigma} \cdot \mathbf{F}^{-T} + \mathbf{F}^{-1} \cdot \frac{d\boldsymbol{\sigma}}{dt} \cdot \mathbf{F}^{-T} + \mathbf{F}^{-1} \cdot \boldsymbol{\sigma} \cdot \frac{d\mathbf{F}^{-T}}{dt} \right]_{ij}, \tag{1.70}$$

and, after using Eq. (1.65) and rearranging, we obtain

$$\frac{d\hat{\sigma}^{ij}}{dt} = \left[\mathbf{F}^{-1} \cdot \left(\frac{\partial \boldsymbol{\sigma}}{\partial t} + \mathbf{u} \cdot \nabla \boldsymbol{\sigma} - (\nabla \mathbf{u})^T \cdot \boldsymbol{\sigma} - \boldsymbol{\sigma} \cdot \nabla \mathbf{u} \right) \cdot \mathbf{F}^{-T} \right]_{ij}, \tag{1.71}$$

where we have used Eq. (1.2) for the total time derivative of $\sigma_{mn}(\mathbf{x}(\mathbf{a},t),t)$. We observe here that Eq. (1.71) has the same structure as the transformation laws, Eq. (1.68), and therefore $d\hat{\sigma}^{ij}/dt$ and the terms in the brackets on the right hand side are components of a second-rank tensor in the corresponding coordinate systems. Therefore,

$$\overset{\triangledown}{\boldsymbol{\sigma}} \equiv \frac{\partial \boldsymbol{\sigma}}{\partial t} + \mathbf{u} \cdot \nabla \boldsymbol{\sigma} - (\nabla \mathbf{u})^T \cdot \boldsymbol{\sigma} - \boldsymbol{\sigma} \cdot \nabla \mathbf{u} \tag{1.72}$$

is a second-rank tensor, and it is a time derivative of the second-rank tensor $\boldsymbol{\sigma}$ embedded in a fluid with the velocity field $\mathbf{u}$. In a similar fashion, considering $d\hat{\sigma}_{ij}/dt$, we arrive at another tensorial formulation of the full-time derivative:

$$\overset{\triangle}{\boldsymbol{\sigma}} \equiv \frac{\partial \boldsymbol{\sigma}}{\partial t} + \mathbf{u} \cdot \nabla \boldsymbol{\sigma} + \boldsymbol{\sigma} \cdot (\nabla \mathbf{u})^T + \nabla \mathbf{u} \cdot \boldsymbol{\sigma}. \tag{1.73}$$

Equations (1.72) and (1.73) define the so-called *upper-convected* and *lower-convected* derivatives of a second-rank tensor. Time derivatives in constitutive relations are generally in one of these two forms in order to ensure that the relation is frame-invariant; other choices of frame-invariant time derivatives are possible (e.g., the so-called *Jaumann* or corotational derivative), but the most popular polymeric constitutive equations are formulated in terms of the upper- and lower-convected derivatives only.

4.3 Canonical Nonlinear Differential Constitutive Equations

4.3.1 A Cooking Recipe

As we have seen in the previous sections, not all combinations of stress and velocity gradient tensors result in physically meaningful equations. It was demonstrated, for example, that a term $d\sigma_{mn}/dt$, where σ_{mn} are the Cartesian coordinates of the stress tensor, can only enter a constitutive equation in a combination with other terms given by the upper- or lower-convected derivatives, Eqs. (1.72) and (1.73). Here we extend this argument and present general principles for formulating a physically admissible constitutive equation. For polymer flows these principles were first formulated by J. Oldroyd and are extensively discussed by Bird et al. [13]. They consist of three main requirements:

- An admissible equation should be frame-invariant.
- The stress tensor $\boldsymbol{\sigma}(t)$ can depend only on the past deformations, $t' < t$, and not on the future $t' > t$.
- Equations should be local in space, i.e., stresses should not depend on the stresses and velocities in the neighboring fluid elements, save through their continuity at the interfaces.

These conditions severely restrict the form of an admissible constitutive equation. Essentially, they imply that such an equation can only be written in terms of functions of frame-invariant combinations of stress and velocity gradient tensors (or, more generally, deformation tensors), as well as their spatial gradients and convected time derivatives. Unfortunately, while eliminating a large number of possible equations, these conditions do not sufficiently restrict the form of the constitutive relation and there is no unique equation that describes viscoelastic polymer solutions similar to the Navier–Stokes equation for Newtonian fluids.

When modeling polymer solutions there are two classes of modeling strategies that one can adopt. The first approach is based on a combination of field-theoretical/symmetry arguments and experimental input. As a first step, one selects a particular order of approximation; for instance, only terms that are at most quadratic in the stress and velocity gradient tensors are considered. Next, the constitutive relation is expressed as a linear combination of these terms with unknown coefficients. Finally, one uses experimentally determined rheological properties in various types of flows to determine whether the equation is sufficient to describe the behavior observed and to fix the values of the unknown coefficients. There is a degree of art involved in this procedure since it is a priori unclear which allowed terms should be included in the model constitutive equation. However, at moderately weak and slow deformations, one would expect only moderate stresses and, hence, the approach outlined above can be seen as using a Taylor expansion to construct successive approximations to the true constitutive law.

The second modeling strategy is to build upon a kinetic theory. Assuming a particular model for polymer molecules, their self-interactions and interactions with other molecules, and their behaviors under flow, one can derive a hydrodynamic

equation relating the macroscopic stress and velocity gradient tensors (albeit often only by using rather uncontrolled approximations). Obviously, this approach cannot produce an equation that is not generated through the first modeling strategy. Indeed, this would imply that the "new" terms somehow do not satisfy the admissibility conditions outlined above and, hence, the resulting equation is unphysical. The strength of this approach is that it provides a microscopic basis for the arbitrary coefficients introduced by the first approach. It also allows one to build up intuition as to how particular molecular models project onto macroscopic constitutive equations.

In the next section we will discuss several popular models constructed with the first strategy, while in Sect. 4.4 we will use the second strategy and develop a macroscopic model for a dilute solution of noninteracting dumbbells using a kinetic theory.

4.3.2 Constitutive Equations from Field-Theoretical and Symmetry Arguments

The simplest class of equations for viscoelastic solutions involves the expression of the stress tensor as a sum of all admissible combinations of the velocity gradient tensor. Depending on the highest algebraic power of the velocity gradient tensor involved, they are called the *second-order fluid*, *third-order fluid*, etc. For example, the deviatoric stress of the second-order fluid is given by

$$\boldsymbol{\tau} = \eta\dot{\boldsymbol{\gamma}} + b_2\overset{\triangledown}{\dot{\boldsymbol{\gamma}}} + b_{11}\dot{\boldsymbol{\gamma}}\cdot\dot{\boldsymbol{\gamma}} \qquad \textit{(second-order fluid)}, \tag{1.74}$$

where η is the total viscosity of the solution, b_2 and b_{11} are material constants, and the triangle denotes the upper-convected derivative, Eq. (1.72). As is clear by observation of Eq. (1.74), the highest-order nonlinearity is quadratic in the velocity gradient, accounting for the name of the model. We also see that model materials of this class exhibit nonlinear responses to applied deformations but have no memory of past stresses and therefore should only be used in situations where the flow changes on time scales significantly longer than the polymer relaxation time. In fact, as we will show later on in Sect. 6, the second-order model is unphysical in any time-dependent flow and should only be used in weak stationary flows.

The simplest equations that take the relaxation of the stress into account are produced by writing a frame-invariant analogue of the linear Maxwell model, already discussed in Sects. 4.1 and 4.2. By choosing either the upper- or lower-convected derivative for the full-time derivative in Eq. (1.54) we arrive at

$$\boldsymbol{\sigma} = -p\mathbf{I} + \boldsymbol{\tau}_p, \tag{1.75}$$

where the polymeric contribution to the stress $\boldsymbol{\tau}_p$ obeys

$$\boldsymbol{\tau}_p + \lambda \overset{\triangledown}{\boldsymbol{\tau}}_p = \eta_p \dot{\boldsymbol{\gamma}} \qquad \textit{(upper-convected Maxwell)}, \tag{1.76}$$

$$\boldsymbol{\tau}_p + \lambda \overset{\triangle}{\boldsymbol{\tau}}_p = \eta_p \dot{\boldsymbol{\gamma}} \qquad \textit{(lower-convected Maxwell)}. \tag{1.77}$$

Here λ is the polymer relaxation time introduced in Sect. 4.1 and η_p is the polymer contribution to the viscosity. Alternatively, one can use a linear combination of the upper- and lower-convected derivatives in the Maxwell model to obtain the so-called *Johnson–Segalman* equation

$$\boldsymbol{\tau}_p + \lambda \left(\frac{1+a}{2} \overset{\triangledown}{\boldsymbol{\tau}}_p + \frac{1-a}{2} \overset{\triangle}{\boldsymbol{\tau}}_p \right) = \eta_p \dot{\boldsymbol{\gamma}} \qquad \textit{(Johnson–Segalman)}. \tag{1.78}$$

The *slip parameter* a ($a \in [-1,1]$) sets the relative importance of the two objective time derivatives derived in Sect. 4.2. Despite their apparent similarities, Eqs. (1.76)–(1.78) produce very different rheological predictions. While the UCM model can capture the properties of many dilute polymer solutions to a relatively good first approximation, the rheological predictions of the lower-convected Maxwell (LCM) model are in strong qualitative disagreement with experimental observations and this model is not generally used. The Johnson–Segalman model predicts non-monotonic behavior of the shear stress with the shear rate in simple shear flows for a wide range of the model parameters and is also not usually used to describe polymeric systems. Instead, it is often employed as a model for shear-banding in wormlike micellar solutions together with the Giesekus model to be introduced shortly [11, 12].

Often a Newtonian stress with a viscosity η_s is added to the total stress in Eq. (1.75):

$$\boldsymbol{\sigma} = -p\mathbf{I} + \eta_s \dot{\boldsymbol{\gamma}} + \boldsymbol{\tau}_p. \tag{1.79}$$

If $\boldsymbol{\tau}_p$ obeys the UCM model, the resulting set of equations is called the *Oldroyd-B* model. The Oldroyd-B model is often formulated in terms of the total deviatoric stress, $\boldsymbol{\tau} = \eta_s \dot{\boldsymbol{\gamma}} + \boldsymbol{\tau}_p$, which satisfies

$$\boldsymbol{\tau} + \lambda \overset{\triangledown}{\boldsymbol{\tau}} = \eta \left(\dot{\boldsymbol{\gamma}} + \lambda_r \overset{\triangledown}{\dot{\boldsymbol{\gamma}}} \right) \qquad \textit{(Oldroyd-B)}, \tag{1.80}$$

where $\eta = \eta_s + \eta_p$ is the total viscosity. The so-called *retardation* time λ_r is not an independent time scale, but is in fact a combination of the Maxwell relaxation time λ and the solvent and polymeric viscosities, $\lambda_r = \lambda(\eta_s/\eta)$. One drawback of the viscoelastic models above is that tensile stresses can grow without bound in

extensional flows. As will be made clear in Sect. 4.4, this can be understood as a continuous stretching of polymers in the flow and an unbounded Hookean stress response.

In the spirit of including all possible tensorial invariants up to a particular order, one can generalize this equation to the so-called *Oldroyd 8-constant* model given by the following constitutive equation:

$$\begin{aligned}\boldsymbol{\tau}+\lambda_1\overset{\triangledown}{\boldsymbol{\tau}}+\lambda_2\left(\dot{\boldsymbol{\gamma}}\cdot\boldsymbol{\tau}+\boldsymbol{\tau}\cdot\dot{\boldsymbol{\gamma}}\right)+\lambda_3\mathrm{Tr}\left(\boldsymbol{\tau}\right)\dot{\boldsymbol{\gamma}}+\lambda_4\left(\boldsymbol{\tau}:\dot{\boldsymbol{\gamma}}\right)\mathbf{I}\\ =\eta\left(\dot{\boldsymbol{\gamma}}+\lambda_5\overset{\triangledown}{\dot{\boldsymbol{\gamma}}}+\lambda_6\dot{\boldsymbol{\gamma}}\cdot\dot{\boldsymbol{\gamma}}+\lambda_7\left(\dot{\boldsymbol{\gamma}}:\dot{\boldsymbol{\gamma}}\right)\mathbf{I}\right)\quad\textit{(Oldroyd 8-constant)},\end{aligned}\tag{1.81}$$

where $\mathrm{Tr}\left(\mathbf{A}\right)$ is the trace of $\mathbf{A}$ and $\mathbf{A}:\mathbf{B}=\sum_{i,j}A_{ij}B_{ji}$ as before. The time scales $\lambda_1\ldots\lambda_7$ and the total viscosity η are the model parameters that are usually determined from experiments. This model covers a wide range of possible rheological predictions and, in principle, can be used to describe a variety of viscoelastic systems. In practice, this is prevented by the large number of model parameters that usually cannot all be fixed by standard rheological measurements. Even in theoretical studies, determining the predictions of the Oldroyd 8-constant model requires a scan of a very large space of possible parameter values and is also not practical. The Oldroyd-B model is a special case of the Oldroyd 8-constant model, partially capturing numerous important viscoelastic phenomena but with many fewer parameters, and is a popular model among experimentalists and theoreticians.

Another class of models is formed by adding various terms nonlinear in $\boldsymbol{\tau}_p$ to the UCM model, Eq. (1.76). One example of such models is the Giesekus equation,

$$\boldsymbol{\tau}_p+\lambda\overset{\triangledown}{\boldsymbol{\tau}}_p+\alpha\frac{\lambda}{\eta_p}\boldsymbol{\tau}_p\cdot\boldsymbol{\tau}_p=\eta_p\dot{\boldsymbol{\gamma}}\qquad\textit{(Giesekus)}.\tag{1.82}$$

Here α is a dimensionless model parameter that should be kept smaller than $1/2$ to avoid a non-monotonic dependence of the shear stress on the shear rate in simple shear flows. Another example is given by the *Phan–Thien–Tanner* (PTT) model,

$$f\left(\boldsymbol{\tau}_p\right)\boldsymbol{\tau}_p+\lambda\overset{\triangledown}{\boldsymbol{\tau}}_p=\eta_p\dot{\boldsymbol{\gamma}}\qquad\textit{(PTT)},\tag{1.83}$$

where $f\left(\boldsymbol{\tau}_p\right)$ is a nonlinear function that can be chosen either in its exponential or, more commonly, in its linear form:

$$f\left(\boldsymbol{\tau}_p\right)=\begin{cases}\exp\left\{\dfrac{\lambda\varepsilon}{\eta_p}\mathrm{Tr}\left(\boldsymbol{\tau}_p\right)\right\} & \text{(exponential)},\\[2ex] 1+\dfrac{\lambda\varepsilon}{\eta_p}\mathrm{Tr}\left(\boldsymbol{\tau}_p\right) & \text{(linear)}.\end{cases}\tag{1.84}$$

The dimensionless parameter ε controls how fast the effective polymeric viscosity and the relaxation time decrease with the stress.

Other constitutive relations were developed to correct the unphysical behavior in the Oldroyd-B and similar models, the so-called finite-extensibility-nonlinear-elastic (FENE) models. These models are comprised of various approximations to the kinetic theory of the FENE model to be discussed in the following section. The two most commonly used models of this type are the FENE-CR model (suggested by Chilcott and Rallison [16]) and the FENE-P model (a Gaussian closure of the kinetic theory model suggested by Peterlin [17]):

$$\boldsymbol{\tau}_p + \lambda \left(\frac{\overset{\triangledown}{\boldsymbol{\tau}_p}}{f(\boldsymbol{\tau}_p)} \right) = \eta_p \dot{\boldsymbol{\gamma}} \qquad (\textit{FENE-CR}) \tag{1.85}$$

and

$$\boldsymbol{\tau}_p + \lambda \left(\frac{\overset{\triangledown}{\boldsymbol{\tau}_p}}{f(\boldsymbol{\tau}_p)} \right) = \frac{\eta_p}{f(\boldsymbol{\tau}_p)} \dot{\boldsymbol{\gamma}} - \eta_p \frac{D}{Dt} \left(\frac{1}{f(\boldsymbol{\tau}_p)} \right) \mathbf{I} \quad (\textit{FENE-P}). \tag{1.86}$$

In the equations above the upper-convected derivatives act on the entire parenthetical expressions, and the function f is given by

$$f(\boldsymbol{\tau}_p) = 1 + \frac{\lambda}{\eta_p L^2} \mathrm{Tr}(\boldsymbol{\tau}_p), \tag{1.87}$$

where L is a dimensionless parameter related to the maximum possible extension of polymer chains. There are several versions of these models in the literature, but in the limit of large L they all reduce to Eqs. (1.85) and (1.86) above.

Finally we introduce the *Rolie-Poly* model, which in its simplest form is given by

$$\boldsymbol{\tau}_p + \lambda \overset{\triangledown}{\boldsymbol{\tau}}_p = \eta_p \dot{\boldsymbol{\gamma}} - \frac{2}{3} \lambda \left(\boldsymbol{\tau}_p : \nabla \mathbf{u} \right) \left(\mathbf{I} + (1+\varepsilon) \frac{\lambda}{\eta_p} \boldsymbol{\tau}_p \right) \quad (\textit{Rolie-Poly}). \tag{1.88}$$

Here again, ε is a dimensionless parameter. The Rolie-Poly model is a relatively new constitutive relation and, as such, has not been studied as much as the other models described in this section. However, it is based on our most detailed molecular picture of polymer solutions and is believed to be one of the best models for concentrated polymeric systems [18].

In this section we have only listed a few popular constitutive models without discussing their physical implications. Some basic predictions of the Oldroyd-B model and how they differ from their Newtonian counterparts will be discussed in Sect. 5. But first, let us turn to the second strategy for developing constitutive laws: using kinetic theories of the polymeric structure and dynamics to build from the ground up.

4.4 A Kinetic Theory: The Linear Elastic Dumbbell Model

In this section we develop a basic kinetic theory for very dilute polymer solutions. Our goal here is to give the reader a taste of how microscopic dynamics of model polymers project onto a particular constitutive equation. In this way we will re-derive the UCM model discussed in Sect. 4.3 and provide relationships between the polymeric viscosity and the relaxation time of the UCM equation and the microscopic properties of polymers.

We begin by considering one of the simplest models of polymer molecules: dumbbells consisting of two beads connected by an elastic spring. Much more intricate models are considered at great length in other texts (see [19–21]), but this simple example remains instructive. The solution of polymers in solvent is assumed to be so dilute that the dumbbells do not affect each other through either hydrodynamic interactions or intermolecular forces. In this setting it is sufficient to consider a single polymer molecule in a background fluid flow, and the total contribution of polymer molecules to the stress of the fluid will simply be a sum of individual contributions. We assume that a spring cannot be bent, i.e., it is always oriented along the line connecting the beads of a dumbbell.

The calculation to follow hinges on a critical separation of scales. Even in very turbulent flows, spatial variations of the velocity field occur over much longer scales than the very small length of a single polymer, and the velocity field "seen" by a single polymer is safely assumed to be linear. Moreover, and importantly, the spatial variation of the velocity field occurs over much longer scales than *very many* polymers. Therefore, in deducing an averaged effect of polymers on the fluid rheology, we need only consider the dynamics of a suspension of polymers in a single linear background flow,

$$\mathbf{u}(\mathbf{x},t) = \mathbf{u}_0 + \mathbf{x}\cdot\mathbf{A}, \tag{1.89}$$

where $\mathbf{u}_0$ is a constant velocity vector and $\mathbf{A} = \nabla\mathbf{u}$ is the (constant) velocity gradient tensor. Finally, as discussed in Sect. 3, there is a significant separation of time and length scales between the polymer and the solvent molecule dynamics, and therefore the polymers are assumed not to disturb the equilibrium properties of the solvent molecules. These are the same assumptions made when considering the Brownian motion of a large particle in a solvent (see Chap. 3). In what follows, the solvent is treated as a heat bath with a large number of degrees of freedom kept at a constant temperature T.

4.4.1 Dumbbell Dynamics and the Smoluchowski Equation

The dumbbell dynamics are found by balancing the forces acting on the two beads. For illustration the beads are assumed to be spherical, and we will not consider the balance of torques. Since the Reynolds number associated with a bead's motion is

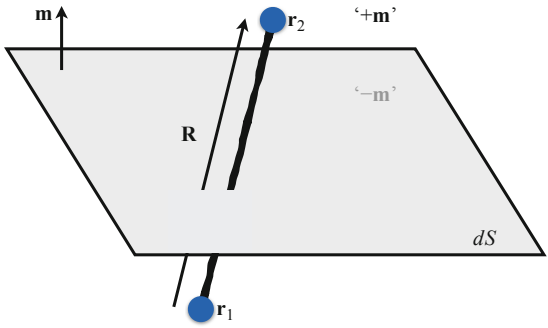

Fig. 1.9 A schematic of the model dumbbell studied in Sect. 4.4 as it passes through an imaginary planar surface with normal vector $\mathbf{m}$. The vector from the first bead (lying in the "$-\mathbf{m}$" half-space) to the second bead (lying in the "$+\mathbf{m}$" half-space) is denoted by $\mathbf{R} = \mathbf{r}_2 - \mathbf{r}_1$. The force exerted by the elastic spring on the first bead is denoted by $\mathbf{F}_s$ and on the second by $-\mathbf{F}_s$

exceptionally small in accordance with its small size, inertia may be safely neglected (see Sect. 2.5). The beads, labeled as "1" and "2", have respective positions $\mathbf{r}_1$, $\mathbf{r}_2$ and velocities $\dot{\mathbf{r}}_1$, $\dot{\mathbf{r}}_2$ (see Fig. 1.9), and the equations of motion are given by

$$\zeta\left(\mathbf{u}\left(\mathbf{r}_1\right) - \dot{\mathbf{r}}_1\right) + \mathbf{F}_s - k_B T \nabla_{\mathbf{r}_1} \ln \Psi = 0, \tag{1.90}$$

$$\zeta\left(\mathbf{u}\left(\mathbf{r}_2\right) - \dot{\mathbf{r}}_2\right) - \mathbf{F}_s - k_B T \nabla_{\mathbf{r}_2} \ln \Psi = 0, \tag{1.91}$$

where the subscript on the gradient operator indicates the variables over which the derivatives are taken, and $\mathbf{u}(\mathbf{x},t) = \mathbf{u}(\mathbf{x})$ from Eq. (1.89). The first term in each equation is the viscous drag on each bead as it moves relative to the flow; the drag coefficient ζ is given by the Stokes drag law, $\zeta = 6\pi\eta_s a$, where η_s is the solvent viscosity and a is the radius of each bead—we have neglected the hydrodynamic interactions between the two beads. The force exerted by the elastic spring on the first bead is denoted by $\mathbf{F}_s$ and on the second by $-\mathbf{F}_s$. The last terms in Eqs. (1.90) and (1.91) are thermodynamic forces exerted by the fluid on the beads, where k_B is the Boltzmann constant. This force has entropic origins and is written in terms of the distribution function $\Psi\left(\mathbf{r}_1, \mathbf{r}_2, t\right)$ that gives the probability of finding the first bead at $\mathbf{r}_1$ and the second bead at $\mathbf{r}_2$ at time t. Below we will provide an intuitive explanation for this particular form of the thermodynamic force.

It is convenient to introduce the position of the center of mass of each dumbbell, $\mathbf{X} = \left(\mathbf{r}_1 + \mathbf{r}_2\right)/2$, and the end-to-end vector, $\mathbf{R} = \mathbf{r}_2 - \mathbf{r}_1$. Since we have assumed a constant velocity gradient, space is homogeneous in our problem (i.e., the polymer "sees" the same velocity gradient $\mathbf{A}$ at each point in space), so that the probability distribution must be independent of the location of the dumbbell. The probability density function may then be written instead as $\Psi = \Psi(\mathbf{R},t)$. Since Ψ is a probability density we require $\int \Psi\left(\mathbf{R},t\right) d^3\mathbf{R} = 1$, and it is assumed to decay sufficiently fast for large $|\mathbf{R}|$.

Adding and subtracting Eqs. (1.90) and (1.91) and using Eq. (1.89), we find

$$\dot{\mathbf{X}} = \mathbf{u}(\mathbf{X}), \tag{1.92}$$

$$\dot{\mathbf{R}} = \mathbf{R}\cdot\mathbf{A} - \frac{2}{\zeta}\mathbf{F}_s(\mathbf{R}) - \frac{2k_BT}{\zeta}\nabla_{\mathbf{R}}\ln\Psi. \tag{1.93}$$

The center of mass is advected by the background flow, while the end-to-end vector evolves in time due to the gradient of the background flow, the spring force, and the thermal fluctuations.

Our next step is to derive an evolution equation for the distribution function Ψ. While such an equation may be derived using a nearly identical approach to that described in Sect. 2.2 (see Chap. 9 for more details), it is more instructive to provide an analogy with the diffusion equation that will allow us to better understand the origin of the terms in Eqs. (1.90) and (1.91). Consider a concentration field $c(\mathbf{x},t)$ of particles suspended in a fluid. The behavior of the concentration is governed by a diffusion equation,

$$\frac{\partial c}{\partial t} + \nabla\cdot\mathbf{J} = 0, \tag{1.94}$$

where the flux $\mathbf{J}$ is given by the familiar Fick's law, $\mathbf{J} = -D\nabla c$, with D a diffusion constant. If an additional force $\mathbf{F}$ is acting on the particles it creates an extra flux $c\mathbf{v}$, where the velocity $\mathbf{v}$ is given by the balance of the force $\mathbf{F}$ and the viscous drag $-\zeta\mathbf{v}$ acting on each particle, and then the total flux can be written as

$$\mathbf{J} = -D\nabla c + \frac{c}{\zeta}\mathbf{F} = \frac{c}{\zeta}\Big(-\zeta D\nabla\ln c + \mathbf{F}\Big). \tag{1.95}$$

Invoking the fluctuation-dissipation theorem one obtains the Stokes-Einstein relation, $\zeta D = k_BT$ (see Chap. 3), and the term in parentheses may be identified as the total force acting on the particle. The first term is an entropic force that acts to remove any concentration gradients in the solution and has the same form as we have used in Eqs. (1.90) and (1.91) if we identify the concentration field c with the probability distribution Ψ.

Analogously, the equation of probability conservation takes the form

$$\frac{\partial\Psi}{\partial t} + \nabla_{\mathbf{R}}\cdot\left(\dot{\mathbf{R}}\,\Psi\right) = 0, \tag{1.96}$$

which is known as the Smoluchowski equation. Upon insertion of Eq. (1.93) into Eq. (1.96) we obtain

$$\frac{\partial \Psi}{\partial t} + \nabla_{\mathbf{R}} \cdot \left\{ \left(\mathbf{R} \cdot \mathbf{A} - \frac{2}{\zeta} \mathbf{F}_s(\mathbf{R}) - \frac{2k_B T}{\zeta} \nabla_{\mathbf{R}} \ln \Psi \right) \Psi \right\} = 0. \tag{1.97}$$

The Smoluchowski equation is nonlinear and in general can only be solved numerically.

4.4.2 The Special Case of the Hookean Dumbbell

Although Eq. (1.97) is analytically intractable in general, for a simple Hookean spring force $\mathbf{F}_s = K\mathbf{R}$, with K a spring constant, a constitutive equation may be derived without knowing the exact form of Ψ. To accomplish this we will require an equation of motion for the average dyadic product of two end-to-end vectors:

$$\langle \mathbf{RR} \rangle \equiv \int \mathbf{RR}\, \Psi(\mathbf{R}, t)\, d^3\mathbf{R}. \tag{1.98}$$

Here the angle brackets denote an ensemble average with the distribution function Ψ. The desired equation of motion is readily obtained by multiplying Eq. (1.97) by $\mathbf{RR}$, taking the ensemble average, and using the following identities (see [21]):

$$\int \mathbf{RR} \frac{\partial \Psi}{\partial t}\, d^3\mathbf{R} = \frac{\partial}{\partial t} \langle \mathbf{RR} \rangle, \tag{1.99}$$

$$\int \mathbf{RR} \nabla_{\mathbf{R}} \cdot (\mathbf{R} \cdot \mathbf{A} \Psi)\, d^3\mathbf{R} = -\mathbf{A}^T \cdot \langle \mathbf{RR} \rangle - \langle \mathbf{RR} \rangle \cdot \mathbf{A}, \tag{1.100}$$

$$\int \mathbf{RR} \nabla_{\mathbf{R}} \cdot (\mathbf{R} \Psi)\, d^3\mathbf{R} = -2 \langle \mathbf{RR} \rangle, \tag{1.101}$$

$$\int \mathbf{RR} \nabla_{\mathbf{R}} \cdot (\nabla_{\mathbf{R}} (\ln \Psi) \Psi)\, d^3\mathbf{R} = 2\mathbf{I}, \tag{1.102}$$

and assuming that the spring force acts only along the axis of the dumbbell, $\mathbf{F}_s = F_s(\mathbf{R})\mathbf{R}$, the resulting equation for the evolution of $\langle \mathbf{RR} \rangle$ is

$$\overset{\nabla}{\langle \mathbf{RR} \rangle} = \frac{4k_B T}{\zeta} \mathbf{I} - \frac{4}{\zeta} \langle \mathbf{RF}_s \rangle. \tag{1.103}$$

In deriving this equation we have used the assumption that Ψ decays sufficiently fast for large $|\mathbf{R}|$ to neglect the boundary terms during the integration by parts. Equation (1.103) implies that in equilibrium, in the absence of flow, we have

$$\langle \mathbf{RF}_s \rangle_{\text{equil}} = k_B T \mathbf{I}. \tag{1.104}$$

4.4.3 Completing the Picture: The Upper-Convected Maxwell Model

We now have the ingredients needed to calculate the polymer contribution to the stress tensor, which will involve measuring the number of dumbbells crossing a given surface and identifying the forces from the stretched dumbbells with the polymeric fluid stress.

To begin, consider an imaginary planar surface in the fluid with area dS and normal vector $\mathbf{m}$ as illustrated in Fig. 1.9. According to the definition given in Sect. 2.4, the traction from the fluid acting on the surface facing in the direction of $\mathbf{m}$ is given by $\mathbf{m}\cdot\boldsymbol{\tau}_p$, which is positive when the resultant force points into the same half-space as $\mathbf{m}$. Consider now a dumbbell with the end-to-end distance $\mathbf{R}$ with its first bead in the "$-\mathbf{m}$" half-space and its second bead in the "$+\mathbf{m}$" half-space, as shown in Fig. 1.9. A dumbbell with the end-to-end distance $\mathbf{R}$ can span both sides of the plane only if its second bead is within a distance $\mathbf{m}\cdot\mathbf{R}$ of the plane and, then depending on that distance, only for a certain range of $\mathbf{R}$. Let n be the number density of dumbbells in the solution. The total number of dumbbells straddling the imaginary surface is then given by $n\,dS\,(\mathbf{m}\cdot\mathbf{R})$.

In the convention we have introduced for the elastic spring, its force $\mathbf{F}_s$ acts on the first bead ($-\mathbf{F}_s$ acts on the second bead). The local force balance on the "$+\mathbf{m}$"-side of the surface implies that the traction on the surface at the point where the end-to-end vector crosses it is equal to $\mathbf{F}_s$. Since the probability of finding a dumbbell in such a configuration is given by $\Psi(\mathbf{R},t)\,d^3\mathbf{R}$, the traction due to this configuration is given by

$$\mathbf{t}^+ = \int_{\mathbf{R}\cdot\mathbf{m}>0} n\,dS\,(\mathbf{m}\cdot\mathbf{R})\,\mathbf{F}_s\,\Psi(\mathbf{R},t)\,d^3\mathbf{R} = n\,dS\,\mathbf{m}\cdot\int_{\mathbf{R}\cdot\mathbf{m}>0}\mathbf{R}\mathbf{F}_s\,\Psi d^3\mathbf{R}, \tag{1.105}$$

where the restriction of the integration domain to $\mathbf{R}\cdot\mathbf{m}>0$ ensures that the beads are in the configuration depicted in Fig. 1.9. On the opposite face of the surface, a similar argument yields the traction there:

$$\mathbf{t}^- = n\,dS\,\mathbf{m}\cdot\int_{\mathbf{R}\cdot\mathbf{m}<0}\mathbf{R}\mathbf{F}_s\,\Psi d^3\mathbf{R}. \tag{1.106}$$

The total traction acting on the imaginary surface is given by the sum of the two tractions above, $\mathbf{t}=\mathbf{t}^+ + \mathbf{t}^- = n\,\mathbf{m}\cdot\langle\mathbf{R}\mathbf{F}_\mathbf{s}\rangle\,dS$. Since the same traction can be written as $\mathbf{m}\cdot\boldsymbol{\tau}_p\,dS$, the polymeric contribution to the stress tensor must be equal to

$$\boldsymbol{\tau}_p = n\langle\mathbf{R}\mathbf{F}_s\rangle - 2nk_BT\mathbf{I}. \tag{1.107}$$

The last term is the isotropic pressure of the ideal gas of the beads, where $2n$ is the number density of the beads, and in the absence of flow this stress tensor does not vanish. Indeed, when $\mathbf{u}=0$,

$$(\boldsymbol{\tau}_p)_{\text{equil}} = n\langle\mathbf{R}\mathbf{F}_s\rangle_{\text{equil}} - 2nk_BT\mathbf{I} = -nk_BT\mathbf{I}, \tag{1.108}$$

using Eq. (1.104). The flow-induced polymeric contribution to the stress tensor is then

$$\boldsymbol{\tau}_p = n\langle \mathbf{R}\mathbf{F}_s \rangle - 2nk_BT\mathbf{I} - (\boldsymbol{\tau}_p)_{\text{equil}} = n\langle \mathbf{R}\mathbf{F}_s \rangle - nk_BT\mathbf{I}. \tag{1.109}$$

Equations (1.97) and (1.109) are the key results of the kinetic theory for dilute solutions of polymers. For a particular choice of the spring law, $\mathbf{F}_s = F_s(\mathbf{R})\,\mathbf{R}$, one would need to solve Eq. (1.97) for the end-to-end distribution function, find the average $\langle \mathbf{R}\mathbf{F}_s \rangle$, and use that result in Eq. (1.109) to find the stress. For the particular case of the Hookean spring law, $\mathbf{F}_s = K\mathbf{R}$, we have $\langle \mathbf{R}\mathbf{F}_s \rangle = K\langle \mathbf{R}\mathbf{R} \rangle$, and we can use Eqs. (1.109) and (1.98) to eliminate $\langle \mathbf{R}\mathbf{R} \rangle$. At last we have reached the final result. Identifying a relaxation time $\lambda = \zeta/(4K)$ and polymer viscosity $\eta_p = \lambda nk_BT$, the polymeric stress above satisfies the following equation:

$$\boldsymbol{\tau}_p + \lambda \overset{\triangledown}{\boldsymbol{\tau}}_p = \eta_p \dot{\boldsymbol{\gamma}}. \tag{1.110}$$

As discussed in Sect. 4.3, kinetic theories cannot produce new types of constitutive equations. Instead, they provide connections between a particular type of molecular theory and a constitutive law and give expressions for the parameters in terms of molecular properties. In the particular case considered here, we have shown that a dilute solution of Hookean dumbbells is described by the UCM model.

The reader should take care to note that the opposite point of view is incorrect: the fact that a particular solution is well described by the UCM model does not necessarily imply that one is dealing with a very dilute solution that consists of approximately Hookean springs. The reason why this statement is incorrect is that the UCM model is one of the simplest frame-invariant models, and many types of kinetic theories project (at least for weak flows) onto that model. In other words, for small deformations, a constitutive equation for polymer solutions almost cannot be anything else save for a few special cases. One possible way of thinking about this is based on one of the central concepts from solid state physics. There it is shown that excitations of a complicated lattice of point-like masses connected by elastic springs can be described as noninteracting degrees of freedom (phonons) that all perform independent harmonic motion with various frequencies. Although these degrees of freedom involve many particles moving in a complicated fashion, these effective degrees of freedom are decoupled from each other. In a similar fashion, for small deformations, one can think of an entangled polymer solution as a dilute solution of *effectively noninteracting* elastic degrees of freedom, each of which involves a significant number of polymers. In turn, this dilute "solution" of the effective degrees of freedom corresponds to the UCM model where the role of dumbbells is played by the collective excitations (normal modes).

5 Material Properties of Viscoelastic Fluids

5.1 Normal Stress Differences

In this section we will discuss the rheological predictions of some of the constitutive models introduced in this chapter. We will show that in a viscoelastic fluid, unlike in a Newtonian fluid, even a two-dimensional shear flow commonly gives rise not only to the off-diagonal elements of the stress tensor (shear stresses), but also to the diagonal components, the normal stresses. Many of the surprising phenomena seen in the flow of complex fluids, and in viscoelastic fluids in particular, can be understood by an examination of these normal stresses and the normal stress differences. We will also show that in shear flows with curved streamlines, normal stresses generate extra forces that are directed towards the center of curvature, pushing fluid elements from their streamlines.

The general mechanism of normal stress development, if not the details which are fluid dependent, is simple to understand and is illustrated in Fig. 1.10a. Polymers are stretched and rotated under the action of the local shear and tend on average to align with the streamlines, while the entropic forces acting to return the molecule to its undisturbed conformation lead to an extra tension in the direction of the flow. Many physical effects attributed to fluid elasticity can be qualitatively understood immediately through this simple concept alone. One of the most famous examples is the Weissenberg effect (viscoelastic rod climbing), illustrated in Fig. 1.10b. A rotating rod in a fluid produces circular streamlines in the flow. In a viscoelastic fluid, polymers align with and stretch along streamlines and respond with a so-called hoop stress (a "strangulation" of the immersed rod, illustrated in Fig. 1.10c, to be discussed). Absent an upper boundary, this response drives the fluid up the rod and out of the bulk. Similar reasoning also accounts for die swell in fluid extrusion and a great number of other fluid phenomena (see a wonderful gallery in [22]). In addition to large-scale collective effects, the presence of normal stress differences in flow can be important on smaller scales as well: cells and other soft biological matter may experience extra polymeric stresses that lead to deformation or possibly rupture.

Each of the many constitutive laws introduced in this chapter comes with its own predictions of normal stress differences, which we shall now investigate using the linear shear flow $\mathbf{u}(\mathbf{x},t) = \mathbf{x}\cdot(\dot{\gamma}\,\mathbf{e}_2\mathbf{e}_1) = (\dot{\gamma}y, 0, 0)$. The first and second normal stress differences, N_1 and N_2, and their coefficients, Ψ_1 and Ψ_2, are defined as

$$N_1 = \tau_{11} - \tau_{22} = \Psi_1\dot{\gamma}^2, \quad N_2 = \tau_{22} - \tau_{33} = \Psi_2\dot{\gamma}^2. \tag{1.111}$$

The first normal stress difference monitors the variation in normal stress between the direction of flow (where tension along streamlines is expected as illustrated in Fig. 1.10) and the direction of shear. The first normal stress difference is usually positive in viscoelastic flows, $\Psi_1 > 0$. The second normal stress difference monitors the stress difference in the two directions normal to the flow direction and is,

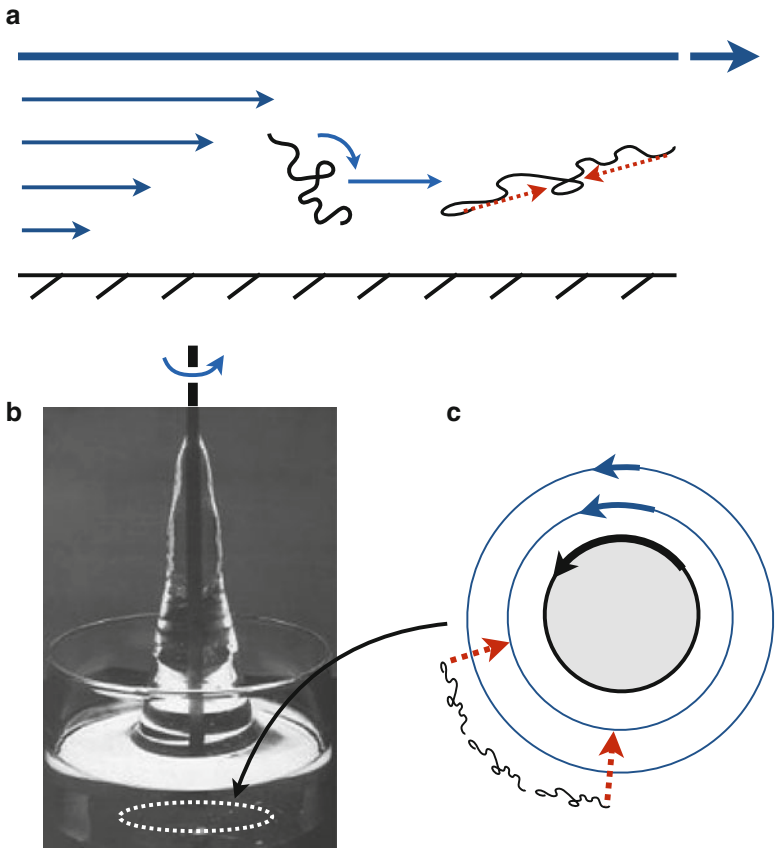

Fig. 1.10 (**a**) An illustration of the mechanism of normal stress differences in viscoelastic fluids. A shear flow rotates and stretches polymers along streamlines creating anisotropic elastic stresses. (**b**) The Weissenberg effect (rod climbing): a rotating rod inside of a viscoelastic fluid excites an upward climb of fluid, unlike in a Newtonian flow (adapted from [22] with permission). (**c**) The Weissenberg effect is explained by normal stress differences, here by the development of hoop stresses along curved streamlines, leading to "strangulation" and an upward ascent

generally, negative and very small compared to the first normal stress difference. Normal stress differences in a general flow may be pronounced near boundaries, including the boundaries of immersed bodies, as the no-slip velocity boundary condition and/or stagnation points of the flow generally introduce a shear flow local to the boundary surface.

In a Newtonian shear flow the pressure is constant, $p = p_0$ [found by inserting the velocity field into Eqs. (1.21) and (1.22)], and the deviatoric stress is

$$\boldsymbol{\tau} = \mu \dot{\boldsymbol{\gamma}} = \mu \dot{\gamma} (\mathbf{e}_2 \mathbf{e}_1 + \mathbf{e}_1 \mathbf{e}_2), \tag{1.112}$$

so that clearly $\Psi_1 = \Psi_2 = 0$. In fact there are no normal stresses whatsoever outside of the constant isotropic pressure in this case, let alone normal stress differences. It is a short exercise to find that there are no normal stress differences associated with the generalized Newtonian fluids introduced in Sect. 3, but this is in keeping with our physical explanation of the source of normal stress differences described above. The linearly viscoelastic fluids introduced in Sect. 4 also do not predict normal stress differences in a shear flow. In order to capture or predict normal stress differences, we must look to the nonlinear constitutive models of viscoelastic fluids. Interestingly, as we shall see below, the normal stresses are generated by the nonlinear terms in the convected derivatives introduced to ensure frame-invariance, revealing a deep connection between geometry and mechanical properties.

Consider the second-order fluid model described in Sect. 4.3. The coefficients in the constitutive law, Eq. (1.74), are in fact directly related to the normal stress differences. Inserting the steady shear flow above into the constitutive relation we find that

$$\boldsymbol{\tau} = \eta\dot{\gamma}\left(\mathbf{e}_2\mathbf{e}_1 + \mathbf{e}_1\mathbf{e}_2\right) - 2b_2\dot{\gamma}^2\mathbf{e}_1\mathbf{e}_1 + b_{11}\dot{\gamma}^2\left(\mathbf{e}_1\mathbf{e}_1 + \mathbf{e}_2\mathbf{e}_2\right). \tag{1.113}$$

Unlike in a Newtonian fluid, the nonlinear terms in the second-order model allow for nonzero normal stress differences in the fluid, $\Psi_1 = -2b_2$ and $\Psi_2 = b_{11}$. Hence, if the viscosity and normal stress differences (the *viscometric functions*) have been measured for a particular fluid, they can be used to specify this particular constitutive model directly as

$$\boldsymbol{\tau} = \eta\dot{\boldsymbol{\gamma}} - \frac{\Psi_1}{2}\overset{\triangledown}{\dot{\boldsymbol{\gamma}}} + \Psi_2\dot{\boldsymbol{\gamma}}\cdot\dot{\boldsymbol{\gamma}}. \tag{1.114}$$

We also see from Eq. (1.113) that the second-order fluid model has no shear-dependent viscosity $\tau_{12}/\dot{\gamma} = \eta$ (constant). Shear-dependent viscosity can be captured at the next order in the retarded-motion expansion, (the third-order fluid model), which has the same normal stress differences as in the second-order model. It is common in the literature to see the approximation $-\Psi_2/\Psi_1 = 1/2$, which overestimates the ratio's value as observed in experiments with most fluids, but is of great use in improving the mathematical tractability of the model. For in this case, the effect of viscoelasticity at first order variation away from the Newtonian flow is simply to modify the pressure and not the fluid velocity field (see [13]).

Next, consider the Oldroyd-B model fluid, Eq. (1.80):

$$\boldsymbol{\tau} + \lambda\overset{\triangledown}{\boldsymbol{\tau}} = \eta\dot{\boldsymbol{\gamma}} + \eta_s\lambda\overset{\triangledown}{\dot{\boldsymbol{\gamma}}}. \tag{1.115}$$

Assuming the same steady shear flow, the individual components of the stress are found to be

$$\boldsymbol{\tau} = 2\lambda\eta_p\dot{\gamma}^2\mathbf{e}_1\mathbf{e}_1 + \eta\dot{\gamma}(\mathbf{e}_1\mathbf{e}_2 + \mathbf{e}_2\mathbf{e}_1) \tag{1.116}$$

(recall that $\eta = \eta_s + \eta_p$). Hence, the first normal stress difference coefficient is $\Psi_1 = 2\lambda\eta_p\,(\geq 0)$. The first normal stress difference is linear in the polymer relaxation time, λ, and vanishes in the limit $\eta_p \to 0$. In the Oldroyd-B model there are no transverse normal stresses in a shear flow, $\tau_{22} = \tau_{33} = 0$, and then trivially $\Psi_2 = 0$. In this model as well we see that the viscosity is always equal to the zero-shear-rate viscosity, $\tau_{12}/\dot{\gamma} = \eta$ (constant). This prediction is inconsistent with experimental observations, in that the viscosity of real polymer solutions often exhibits shear-thinning. Shear-thinning is, however, successfully captured by other nonlinear models, including the FENE-P, Giesekus, and PTT models discussed in Sect. 4.3.

As we have demonstrated above, the only nontrivial component of the stress tensor that appears in the second-order and Oldroyd-B fluids is τ_{11}. Within the kinetic theory approach, Eq. (1.109) allows us to conclude that this stress component is generated by a nonzero component of the end-to-end tensor $\langle R_1 R_1 \rangle$. In turn, this implies that the polymers are stretched and oriented in the flow direction as described at the beginning of this section. From symmetry arguments, changing the direction of the shear, $\dot{\gamma} \to -\dot{\gamma}$, does not change the polymer stretch and orientation. Hence, τ_{11} and N_1 in general should depend on an even power of $\dot{\gamma}$. As we see in the Oldroyd-B model from Eq. (1.116), $N_1 \sim \dot{\gamma}^2$.

Note that the picture of polymers being stretched and aligned in the direction of flow is only accurate *on average*. Recent simulations [23, 24] of individual dumbbells in shear flows suggest that a dumbbell performs the motion that is similar to the Jeffery orbit of a rod in shear flows [9]: most of the time the dumbbell is oriented at an angle with respect to the flow direction, but it periodically tumbles out of this configuration. The relative time spent tumbling and the angle with respect to the flow direction decrease with the shear rate, while its stretch increases with $\dot{\gamma}$, giving support to the coarse-grained molecular picture discussed above.

5.2 Normal-Stress Measurements

There are a number of ways in which the normal stress differences may be measured in the lab. Oftentimes, the only significant component of the normal stresses in a two-dimensional linear shear flow is τ_{11}. In order to measure it, one has to somehow access the forces exerted by the fluid in the flow direction without disturbing the velocity profile. This is very difficult technically and instead one usually takes advantage of the coupling between the normal stresses and the forces on the boundaries that exist in some curvilinear geometries. One of the most common devices for measuring the material properties of a fluid, or *rheometers*, is the *cone-and-plate* apparatus illustrated in Fig. 1.11. In this device a cone is rotated above a horizontal plate with the fluid under investigation filling the gap between them. The fluid meniscus is exposed to the atmosphere.

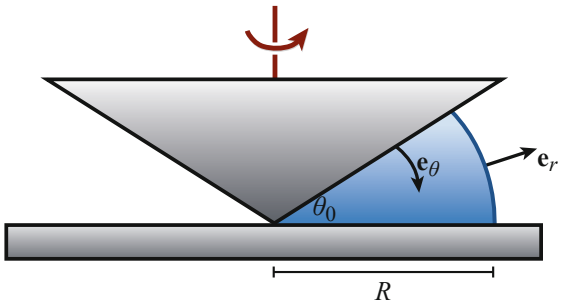

Fig. 1.11 Illustration of a common cone-and-plate rheometer for measuring material properties. The meniscus of the fluid is exposed to the surrounding atmosphere (*the curved blue line*). The geometry is special because the shear rate is uniform throughout the sample

In order to most easily connect the measurements of the cone-and-plate rheometer to the constitutive equations we will assume that the cone touches the plate at a point. The gap between the cone and the plate has the shape of a spherical segment with a small opening angle θ_0, which typically measures only a few degrees. The most convenient way to describe this geometry is to introduce a spherical coordinate system (r, θ, ϕ), with r measuring the distance from the point of contact between the cone and plate. The angle θ is measured from the axis of rotation and the angle ϕ—around that axis, see Fig. 1.11. The fluid fills the gap up to $r = R$. Given the rotational symmetry, the fluid velocity at each point has only one component, u_ϕ, that depends only on the local distance between that point, the cone, and the plate; that position in the gap is set by θ.

The advantages of this geometry are that it is curvilinear (we shall see below why this is important) and that it has a constant shear rate. Indeed, since the angle θ_0 is small, the azimuthal velocity of a point on the cone is given by ωr, where ω is the angular velocity of the cone and r is the radial position of the point. The distance between the cone and the plate at that point is given by $r\theta_0$, which results in the shear rate at that radial distance, ω/θ_0, independent of r! Since the shear rate is the same everywhere, the polymeric stresses may be assumed position-independent in the sample, similar to the case of linear shear considered above.

In what follows, we do not employ any constitutive relation between the polymeric stress and the velocity gradient and only consider the momentum balance equation. Since, typically, polymeric fluids are rather viscous and the measurements are performed at relatively low flow velocities (though the velocity gradients are not small), fluid inertia is generally neglected. The radial component of the momentum balance equation in spherical coordinates then reads

$$-\frac{\partial p}{\partial r} + \frac{1}{r^2}\frac{\partial}{\partial r}\left(r^2 \tau_{rr}\right) - \frac{\tau_{\theta\theta} + \tau_{\phi\phi}}{r} = 0, \tag{1.117}$$

where $\boldsymbol{\tau}$ is the deviatoric stress tensor that has both polymeric and Newtonian solvent contributions and p is the pressure. Using the definition of the first and second normal stress differences, N_1 and N_2, we can write

$$N_1 = \tau_{\phi\phi} - \tau_{\theta\theta}, \qquad N_2 = \tau_{\theta\theta} - \tau_{rr}, \tag{1.118}$$

where the ϕ- and θ-directions have been identified as the flow and gradient directions. Using these definitions in Eq. (1.117) and employing the fact that $\boldsymbol{\tau}$ is constant in space, we obtain

$$-\frac{\partial p}{\partial r} = \frac{2N_2 + N_1}{r}. \tag{1.119}$$

This result is the mathematical foundation of the hoop stresses discussed in the last section: in curved geometries, the tension along the flow lines N_1 is balanced by an inward-pointing pressure gradient that grows in the direction of the origin. In an open geometry, this pressure gradient can result in the rod-climbing effect shown in Fig. 1.10b. Integrating Eq. (1.119), we have

$$-p(r) = -p(R) + (2N_2 + N_1)\ln\frac{r}{R}, \tag{1.120}$$

where the value of the pressure at the meniscus of the cone and plate rheometer, $p(R)$, is an unknown integration constant to be determined. Since the meniscus is in equilibrium, we require that the force per unit area acting on it from the fluid perpendicular to its surface is balanced by the atmospheric pressure p_{atm} from the outside

$$-p(R) + \tau_{rr}(R) + \frac{2\alpha}{R} = p_{\text{atm}}. \tag{1.121}$$

The third term on the l.h.s. is the Laplace pressure under a curved surface and α is the surface tension. Note that the meniscus is the surface of a spherical segment and its principle radii of curvature R_1 and R_2 are the same, $R_1 = R_2 = R$. Force balance, Eq. (1.121), allows us to determine the unknown constant $p(R)$.

The normal force exerted on the plate by the fluid is given by

$$F = 2\pi\int_0^R r\big[-p(r) + \tau_{\theta\theta}\big]\,dr + 2\pi\alpha R. \tag{1.122}$$

The first term is the local fluid stress normal to the plate, $-p(r) + \tau_{\theta\theta}$, integrated over its surface, and the last term is the contribution of the line tension of the meniscus on the plate. The total stress perpendicular to the plate can be rearranged as

$$-p(r) + \tau_{\theta\theta} = (2N_2 + N_1)\ln\frac{r}{R} + p_{\text{atm}} + N_2 - \frac{2\alpha}{R}, \tag{1.123}$$

where we have made use of Eqs. (1.120) and (1.121). After integration, we obtain

$$F = \pi R^2 p_{\text{atm}} - \frac{\pi R^2}{2} N_1 . \tag{1.124}$$

The force acting on the plate from the atmosphere is simply $\pi R^2 p_{\text{atm}}$, and the excess force ΔF is, finally,

$$\Delta F = -\frac{\pi R^2}{2} N_1 . \tag{1.125}$$

This expression provides a simple way of measuring the first normal stress difference by measuring the total force exerted on the plate when the cone is rotating. We note here that this is only possible because of the curvilinear geometry of this setup. As can be seen from Eq. (1.117) or Eq. (1.119), in the limit of a linear shear that is attained by $r \to \infty$, the normal stresses decouple from the pressure gradient and one cannot access N_1 by measuring the force on the plate. A similar argument shows that the normal stresses cannot be measured in the Taylor–Couette geometry (flow in the gap between two rotating coaxial cylinders), but are accessible in another curvilinear geometry, the plate-and-plate setup, that is essentially the cone-and-plate rheometer with the cone replaced by another plate. In that setup, however, the shear rate is not constant everywhere in the sample and it is often difficult to interpret measured quantities.

In practice there are many sources of experimental error, and great care must be taken in interpreting the measured data correctly. Fluid and instrument inertia, secondary flows, elastic instabilities, slip, and many other real issues can lead to Newtonian samples appearing to be complex and vice versa. The derivation of the force exerted by the fluid on the plate, the quantity that is measured by commercial rheometers, helps us to identify potential sources of errors in such experiments. One contribution to the experimental error is due to the instrumental resolution of the pressure transducer used to measure the force, and it is typically rather small. More importantly, the effects of the surface tension in the stress continuity at the meniscus, Eq. (1.121), and the force due to the line tension in Eq. (1.122) strongly depend on the contact angle between the fluid and the walls of the rheometer. In fact, the contact angle between the fluid and the walls of the rheometer can vary from experiment to experiment giving rise to an extra force on the plate that would depend on how the gap was filled with the fluid. Obviously, this extra force has nothing to do with the normal stresses and is a major source of nonsystematic experimental errors. These challenges and others, along with the techniques for reducing errors, are the topic of Chap. 6.

5.3 Other Flows

Besides the simple shear flows discussed above, there are many ways of assessing the material properties of viscoelastic fluids. A natural generalization of the steady two-dimensional shear flow introduces time dependence, $\mathbf{u} = \mathbf{x} \cdot (\dot{\gamma}(t)\mathbf{e}_2\mathbf{e}_1) = (\dot{\gamma}(t)y, 0, 0)$. Using the Oldroyd-B constitutive law as an illustrative example, it is a simple exercise to show that the stress has the form $\boldsymbol{\tau}(t) = \tau_{11}(t)\mathbf{e}_1\mathbf{e}_1 + \tau_{12}(t)(\mathbf{e}_1\mathbf{e}_2 + \mathbf{e}_2\mathbf{e}_1)$ and that the stress components satisfy the following coupled differential equations:

$$\left(1 + \lambda \frac{d}{dt}\right) \tau_{11} - 2\lambda \dot{\gamma}(t)\tau_{12} = -2\eta_s \lambda \dot{\gamma}^2(t), \tag{1.126}$$

$$\left(1 + \lambda \frac{d}{dt}\right) \tau_{12} = \left(\eta + \lambda \eta_s \frac{d}{dt}\right) \dot{\gamma}(t). \tag{1.127}$$

From these expressions the normal stress differences may be predicted for arbitrary time-dependent shear flows. Many experimental apparatuses, including the popular cone and plate, plate and plate, and capillary rheometers, are designed to impose the time dependence of the shear rate and infer material parameters by the forces and torques found in response. Such tests include steady shear, $\dot{\gamma}(t) = \dot{\gamma}_0$; stress growth and relaxation, $\dot{\gamma}(t) = \dot{\gamma}_0 H(t)$ and $\dot{\gamma}(t) = \dot{\gamma}_0 H(-t)$ with $H(t)$ the Heaviside function; step strain, $\dot{\gamma}(t) = \dot{\gamma}_0 (H(t) - H(t - t_0))$ with $t_0 > 0$; and small-amplitude oscillatory shear, $\dot{\gamma} = \dot{\gamma}_0 \sin(\omega t)$ (as discussed in Sect. 4.1). Another common test uses a creep flow, in which an impulsive and constant shear stress is applied to the material and the time dependence of the fluid response is observed. Another method of rheology growing in popularity makes use of large-amplitude oscillatory shear [25–27]. An entirely different approach to measuring material properties makes use of the fluctuations of small probes at the microscale and is termed microrheology. Theoretical microrheology is discussed extensively in Chap. 3 and used as a basis to study the material properties of membranes in Chap. 4.

Other rheometers have been designed to measure the stress-strain responses in another important rheological flow, an extensional flow. A pure extensional flow is written as $\mathbf{u}(\mathbf{x}, t) = \mathbf{x} \cdot (\dot{\varepsilon}\mathbf{e}_1 - \dot{\varepsilon}(\mathbf{e}_2 + \mathbf{e}_3)/2) = \dot{\varepsilon}(x, -y/2, -z/2)$, where $\dot{\varepsilon}$ is the rate of extension, so that $\dot{\boldsymbol{\gamma}} = \dot{\varepsilon}(2\mathbf{e}_1\mathbf{e}_1 - \mathbf{e}_2\mathbf{e}_2 - \mathbf{e}_3\mathbf{e}_3)$. This flow is called extensional since two material points originally close to each other will be separated exponentially in time by this flow as can be seen from the kinematic equations

$$\dot{x}(t) = \dot{\varepsilon}\, x, \qquad \dot{y}(t) = -\frac{\dot{\varepsilon}}{2} y, \qquad \dot{z}(t) = -\frac{\dot{\varepsilon}}{2} z, \tag{1.128}$$

where a dot denotes a time derivative. A commonly measured material response in this setting is called the "extensional viscosity," defined as

$$\bar{\eta} = \frac{\tau_{11} - \tau_{22}}{\dot{\varepsilon}}, \tag{1.129}$$

though the use of the term in time-dependent flows is "fraught with danger" [28]. In a Newtonian fluid, with $\boldsymbol{\tau} = \mu\dot{\boldsymbol{\gamma}}$, we have simply that $\bar{\eta} = 3\mu$. In a second-order fluid we have

$$\bar{\eta} = 3\left(\eta + (b_{11} - b_2)\,\dot{\varepsilon}\right), \tag{1.130}$$

and in an Oldroyd-B fluid,

$$\bar{\eta} = 3\frac{\eta - \eta_s\lambda\dot{\varepsilon} - 2\eta_s\lambda^2\dot{\varepsilon}^2}{(1 - 2\lambda\dot{\varepsilon})\,(1 + \lambda\dot{\varepsilon})}. \tag{1.131}$$

This expression indicates that the stresses grow very rapidly with $\dot{\varepsilon}$ since polymers oppose exponential separation of their ends and, in the case of the Oldroyd-B model, Eq. (1.131), even diverge for $\lambda\dot{\varepsilon} = 1/2$. This phenomenon, sometimes miscalled the *coil-stretch transition*, is the consequence of the unrealistic behavior of the underlying Hookean force law for the dumbbells—their ends can be separated without limits producing very large stresses. Finite extensibility of polymer chains, or other nonlinear mechanisms presented in models like FENE-P, Giesekus, PTT, and others, cures this problem while still exhibiting a rapid growth of $\bar{\eta}$ with $\dot{\varepsilon}$. However, in all of the models above, large extensional stresses and its gradients have proven to be very problematic in the computation of highly elastic flows. Together with the loss of positive definiteness discussed in Sect. 6, it forms the basis of the High-Weissenberg-Number Problem in computational complex fluids in both two and three dimensions. This topic is addressed in detail in Chap. 10.

6 Final Words of Caution: A Health Warning

Modeling complex fluids can be a tricky business. The primary challenges when dealing with the constitutive models described in this chapter generally arise due to their strongly nonlinear nature. Unless these models are used to study simple, steady flows, it is generally impossible to derive analytical solutions. Instead, one is faced with making perhaps severe analytical approximations or performing time-dependent direct numerical simulations. While both strategies have proven to be fruitful in understanding complicated flows of viscoelastic fluids, they both open the door to serious potential pitfalls. To conclude this chapter we will describe several typical problems that can arise in *approximating* solutions to viscoelastic equations of motion, whether the approximation be analytical or numerical.

The Linear Maxwell Model Is Not Objective One of the more common mistakes made is the inappropriate use of the linear Maxwell model, Eq. (1.54), in actual

calculations. It is often argued that studying this model allows one to understand how fluid memory affects the flow, as opposed to normal stress differences, shear-thinning, and other effects that arise from various nonlinear terms in the constitutive models. The trouble with this approach is that the linear Maxwell model, Eq. (1.54), is not frame-invariant and none of the conclusions drawn from studying this model are guaranteed to be physical. The only way to check whether its predictions are physical is to perform an analysis of the full original constitutive model and compare the two results, at which point the analysis of Eq. (1.54) will have become unnecessary. Unless the original constitutive model reduces exactly to the linear Maxwell model (as is the case with the shear-stress equation for the small-amplitude oscillatory shear flow[1]), the use of the linear Maxwell model should be forbidden!

Time-Dependent Flows in Weakly-Nonlinear Viscoelastic Fluids Are Unstable A second common problem arises in studying weakly nonlinear flows of viscoelastic systems. Consider, for instance, the complete Oldroyd-B model equations (see Sect. 4.3):

$$\rho\left(\frac{\partial \mathbf{u}}{\partial t}+\mathbf{u}\cdot\nabla\mathbf{u}\right)=-\nabla p+\nabla\cdot\boldsymbol{\tau}, \tag{1.132}$$

$$\boldsymbol{\tau}+\lambda\overset{\triangledown}{\boldsymbol{\tau}}=\eta\left(\dot{\boldsymbol{\gamma}}+\lambda(\eta_s/\eta)\overset{\triangledown}{\dot{\boldsymbol{\gamma}}}\right), \tag{1.133}$$

$$\nabla\cdot\mathbf{u}=0. \tag{1.134}$$

A weakly nonlinear flow is a situation wherein the flow changes on time scales much longer than the relaxation time, λ, and therefore λ is in some sense small and can be used as an expansion parameter. It is generally a bad practice to perform a Taylor expansion in a dimensional variable; a better expansion parameter might be λ/τ_0, where τ_0 is the typical time scale set by the flow, which becomes apparent when Eqs. (1.132)–(1.134) are written in dimensionless form. Nevertheless, formally we might write

$$\boldsymbol{\tau}=\boldsymbol{\tau}^{(0)}+\lambda\boldsymbol{\tau}^{(1)}+\mathbf{O}(\lambda^2). \tag{1.135}$$

Substituting this expression into Eq. (1.133), at leading order we recover a Newtonian constitutive relation:

$$\boldsymbol{\tau}^{(0)}=\eta\dot{\boldsymbol{\gamma}}, \tag{1.136}$$

(recall that $\eta=\eta_s+\eta_p$), and

$$\boldsymbol{\tau}^{(1)}=-\overset{\triangledown}{\boldsymbol{\tau}}^{(0)}+\eta_s\overset{\triangledown}{\dot{\boldsymbol{\gamma}}}=-\eta_p\overset{\triangledown}{\dot{\boldsymbol{\gamma}}}. \tag{1.137}$$

[1]Note, however, that this coincidence is only partial: for example, equations for the normal components of the stress tensor *do not* reduce to the linear Maxwell equations in the same geometry.

Truncating the $O\left(\lambda^2\right)$ terms in Eq. (1.137), we are thus left with a particular case of the second-order model, Eq. (1.74), where $b_1 = -\lambda\eta_p$ and $b_{11} = 0$. With this in mind, let us consider the more general constitutive relation given by Eq. (1.74).

Consider a two-dimensional shear flow given by $\mathbf{u} = (u(y,t),0)$. Upon insertion into the momentum balance equation Eq. (1.132), and using the second-order fluid model, Eq. (1.74), an equation for the evolution of $u(y,t)$ is found:

$$\rho\frac{\partial u}{\partial t} = \frac{\partial}{\partial y}\tau_{xy}, \tag{1.138}$$

where the shear stress is given by

$$\tau_{xy} = \eta\frac{\partial u}{\partial y} + b_2\frac{\partial}{\partial t}\frac{\partial u}{\partial y}. \tag{1.139}$$

Combining these two equations we find that

$$\rho\frac{\partial u}{\partial t} = \eta\frac{\partial^2 u}{\partial y^2} + b_2\frac{\partial}{\partial t}\frac{\partial^2 u}{\partial y^2}. \tag{1.140}$$

Just as in Sect. 3.3, we take no-slip boundary conditions at the walls of a channel located at $y = 0$ and $y = h$ and write the flow velocity as a Fourier series:

$$u(y,t) = \sum_{m=1}^{\infty} u_m e^{\alpha_m t}\sin\frac{m\pi y}{h}. \tag{1.141}$$

The growth rates α_m associated with each mode are obtained by substituting this expression into Eq. (1.140), revealing

$$\alpha_m = \frac{-\eta}{b_2 + \rho h^2/(m\pi)^2}. \tag{1.142}$$

For polymer solutions b_2 is typically negative (recall its value based on the Oldroyd-B model, $b_2 = -\lambda\eta_p$), so that α_m is positive for sufficiently large m. This implies that a steady shear flow of a second-order fluid is unstable to short-wavelength perturbations and cannot be realized. In the case of negligible inertia, achieved in the above by setting $\rho = 0$, Eq. (1.142) predicts that *all* Fourier modes are unstable. The implications of this result are profound: it shows that an approximation of slow flows, or, in other words, Taylor expansions of the stress in terms of the relaxation time cannot be used in time-dependent flows where any shear component would result locally in a linear instability and exponential growth of the stress. Hence, the second-order fluid and similar approximations should generally not be used to study time-dependent flows!

The Conformation Tensor Must Remain Positive-Semidefinite Finally, we comment on a problem that is often encountered in the numerical solution of viscoelastic flows. We will base our discussion on the UCM model for simplicity, but the conclusions we will reach are much more general. In the kinetic theory outlined in Sect. 4.4, we concluded that the polymeric contribution $\boldsymbol{\tau}_p$ to the stress tensor is related to the dyadic tensor $\langle \mathbf{RR} \rangle$ by

$$\boldsymbol{\tau}_p = nK\langle \mathbf{RR} \rangle - \frac{\eta_p}{\lambda}\mathbf{I}, \tag{1.143}$$

where $\mathbf{R}$ is the end-to-end distance of a polymer molecule that was represented by a dumbbell in Sect. 4.4. To obtain this expression we have used Eq. (1.109) and the molecular expressions for η_p and λ obtained in Sect. 4.4. The tensor $\langle \mathbf{RR} \rangle$ in its dimensionless form is often referred to as the *conformation tensor*. At a given point in an arbitrary flow, the $\langle \mathbf{RR} \rangle$-tensor can be diagonalized, $\langle \mathbf{RR} \rangle = \mathrm{diag}\left(R_1^2, R_2^2, R_3^2\right)$, where R_1, R_2, and R_3 are the projections of the end-to-end vector on the corresponding coordinate axes. Since the diagonal entries are the *squares* of these projections, they cannot be negative in any flow if the $\langle \mathbf{RR} \rangle$-tensor is to remain physical. Since, by construction, R_1^2, R_2^2, and R_3^2 are the eigenvalues of the $\langle \mathbf{RR} \rangle$-tensor at the considered point in space and time, this statement translates into the requirement that the eigenvalues of the $\langle \mathbf{RR} \rangle$-tensor always remain nonnegative in the whole domain considered.

Although we have introduced this requirement based on the kinetic theory, it is more general. Even if nothing is stated about the physical meaning of the $\langle \mathbf{RR} \rangle$-tensor, it can be formally introduced through, say, Eq. (1.143) (if one deals with the Oldroyd-B model) and it is then possible to prove that if at time t_0 the eigenvalues of $\langle \mathbf{RR} \rangle$ are nonnegative everywhere in the domain, they remain nonnegative for all later times. This property is often referred to as the *evolutionary* nature of the corresponding constitutive equation and has been proven for the Oldroyd-B (UCM), Giesekus, and other models [29]. Since the rest state with no stress is clearly positive-semidefinite (its eigenvalues are not negative), any time evolution starting from this state should remain positive-semidefinite. Unfortunately, this is not the case in both simulations and analytic calculations involving approximations.

Often, due to either accumulation of numerical errors or a severe approximation the conformation tensor may develop negative eigenvalues and become unphysical. Unfortunately, the constitutive equations that have been used in this chapter do not provide a clear indicator of when this will happen (i.e., the stress values do not suddenly diverge at this point or similar). In order to ensure that the results are physical it is therefore advisable to check that the conformation tensor is positive-semidefinite in the whole domain at each time-step in simulations or at the end of analytical calculations. If the conformation tensor is ever found not to be positive-semidefinite, the resulting calculation should not be trusted!

7 Conclusion

In this chapter we presented the fundamental concepts in continuum mechanics and laid the foundations for the mathematical modeling of complex fluids. Numerous constitutive models were introduced, each used to describe complex fluid phenomena such as shear-dependent viscosity and viscoelasticity at varying levels of sophistication. The importance of frame-invariance was stressed in the path to developing mathematically and physically sound nonlinear models including the upper-convected Maxwell (UCM) and Oldroyd-B models and others. Kinetic theory was used as an alternate means of deriving a constitutive law, namely the UCM model, from the ground up. Finally, normal stress differences were discussed, and warnings were given about common dangers encountered in the mathematical modeling of complex fluids.

There are great challenges that remain in the study of complex fluid flows in biological systems. The mathematical modeling of real biological materials by a careful selection of constitutive relation remains problem dependent and is a delicate art. Some of the most popular constitutive laws, such as the Oldroyd-B model of viscoelastic fluids, still present challenges to mathematical analysis and even numerical simulation of highly elastic fluid flows. We may have made great strides in understanding how complex fluid flows change the behavior of immersed soft biological structures, from individual cells to motile microorganisms, but we have barely scratched the surface when it comes to understanding the evolution of biological materials and organisms in the context of non-Newtonian fluid environments. There is much yet to learn in this very exciting convergence of fields.

References

1. G.K. Batchelor, *An Introduction to Fluid Dynamics* (Cambridge University Press, Cambridge, 2000)
2. L.D. Landau, E.M. Lifshitz, *Fluid Mechanics* (translated from Russian by J.B. Sykes and W.H. Reid), vol. 6 (Butterworth-Heinemann, Oxford, 1987)
3. L.G. Leal, *Advanced Transport Phenomena: Fluid Mechanics and Convective Transport Processes*, vol. 7 (Cambridge University Press, Cambridge, 2007)
4. C. Pozrikidis, *Introduction to Theoretical and Computational Fluid Dynamics* (Oxford University Press, Oxford, 2011)
5. D.J. Acheson, *Elementary Fluid Dynamics* (Oxford University Press, Oxford, 1990)
6. S. Childress, *An Introduction to Theoretical Fluid Mechanics* (Courant Lecture Notes) (American Mathematical Society, Courant Institute of Mathematical Sciences at New York University, 2009)
7. C. Pozrikidis, *Boundary Integral and Singularity Methods for Linearized Viscous Flow* (Cambridge University Press, Cambridge, 1992)
8. I.Z. Fisher, *Statistical Theory of Liquids* (University of Chicago Press, Chicago, 1961)
9. R.G. Larson, *The Structure and Rheology of Complex Fluids* (Oxford University Press, Oxford, 1999)

10. D.R. Foss, J.F. Brady, J. Rheol. **44**, 629 (2000)
11. M.E. Cates, S.M. Fielding, Adv. Phys. **55**, 799 (2006)
12. S. Lerouge, J.F. Berret, Adv. Polym. Sci. **230**, 1 (2010)
13. R.B. Bird, C.F. Curtiss, R.C. Armstrong, O. Hassager, *Dynamics of polymeric liquids*, vol. 1, *Fluid Mechanics*, 2nd edn. (Wiley, New York, 1987)
14. A. Lodge, *Elastic Liquids: An Introductory Vector Treatment of Finite-Strain Polymer Rheology* (Academic, New York, 1964)
15. L. Sedov, *Introduction to the Mechanics of a Continuous Medium*. ADIWES International Series in the Engineering Sciences (Addison-Wesley, Reading, 1965)
16. M. Chilcott, J. Rallison, J. Non-Newtonian Fluid Mech. **29**, 381 (1988)
17. A. Peterlin, J. Polym. Sci. Part B Polym. Phys. **4**, 287 (1966)
18. A.E. Likhtman, R.S. Graham, J. Non-Newtonian Fluid Mech. **114**, 1 (2003)
19. R.B. Bird, C.F. Curtiss, R.C. Armstrong, O. Hassager, *Dynamics of polymeric liquids*, vol. 2, *Kinetic Theory*, 2nd edn. (Wiley, New York, 1987)
20. M. Doi, S. Edwards, *The Theory of Polymer Dynamics* (Oxford University Press, Oxford, 1986)
21. R.G. Larson, *Constitutive Equations for Polymer Melts and Solutions* (Butterworths, Boston, 1988)
22. D.V. Boger, K. Walters, *Rheological Phenomena in Focus* (Elsevier, Amsterdam, 1993)
23. A. Celani, A. Puliafito, K. Turitsyn, Europhys. Lett. **70**, 464 (2005)
24. E. Sultan, J.W. van de Meent, E. Somfai, A.N. Morozov, W. van Saarloos, Europhys. Lett. **90**, 99–121 (2010)
25. A.J. Giacomin, J.M. Dealy, *Techniques in Rheological Measurement* (Springer, New York, 1993)
26. R.H. Ewoldt, A. Hosoi, G.H. McKinley, J. Rheol. **52**, 1427 (2008)
27. K. Hyun, M. Wilhelm, C.O. Klein, K.S. Cho, J.G. Nam, K.H. Ahn, S.J. Lee, R.H. Ewoldt, G.H. McKinley, Prog. Polym. Sci. **36**, 1697 (2011)
28. C.J. Petrie, J. Non-Newtonian Fluid Mech. **137**, 15 (2006)
29. M.A. Hulsen, J. Non-Newtonian Fluid Mech. **38**, 93 (1990)